Plankton food webs in the oligotrophic Gulf of Mexico spawning grounds of Atlantic Bluefin tuna

MICHAEL R. STUKEL^{1,2,*}, TRIKA GERARD³, THOMAS KELLY¹, ANGELA N. KNAPP¹, RAÚL LAIZ-CARRIÓN⁴, JOHN T. LAMKIN³, MICHAEL R. LANDRY⁵, ESTRELLA MALCA⁶, KAREN E. SELPH⁷, AKIHIRO SHIROZA⁶, TAYLOR A. SHROPSHIRE^{1,2}, RASMUS SWALETHORP⁵

¹ Earth, Ocean, and Atmospheric Science, Florida State University, Tallahassee, FL 32306, USA, ² Center for Ocean-Atmosphere Prediction Studies, Florida State University, Tallahassee, FL 32306, USA, ³ Southeast Fisheries Science Center, National Marine Fisheries Service, National Oceanic and Atmospheric Administration (NOAA), Miami, FL 33149, USA, ⁴ Centro Oceanografico de Malaga, Instituto Español del Oceanografia, Fuengirola, Spain, ⁵ Scripps Institution of Oceanography, La Jolla, CA 92093, USA, ⁶ Cooperative Institute for Marine and Atmospheric Studies, University of Miami, Miami, FL 33149, USA, ⁷ Department of Oceanography, University of Hawaii at Manoa, Honolulu, HI 96822, USA

*CORRESPONDING AUTHOR: mstukel@fsu.edu

Key words: plankton ecology, marine food web, calanoid copepods, larval fish, nitrogen cycle

ABSTRACT

We used linear inverse ecosystem modeling techniques to assimilate data from extensive Lagrangian field experiments into a mass-balance constrained food web for the Gulf of Mexico open-ocean ecosystem. This region is highly oligotrophic, yet Atlantic Bluefin Tuna (ABT) travel long distances from feeding grounds in the North Atlantic to spawn there. Our results show extensive nutrient regeneration fueling primary productivity (mostly by cyanobacteria and other picophytoplankton) in the upper euphotic zone. The food web is dominated by the microbial loop (>70% of net primary productivity is respired by heterotrophic bacteria and protists that feed on them). In contrast, herbivorous food web pathways from phytoplankton to metazoan zooplankton process <10% of net primary production in the mixed layer. Nevertheless, ABT larvae feed preferentially on podonid cladocerans and other suspensionfeeding zooplankton that in turn derive much of their nutrition from nanoand micro-phytoplankton (mixotrophic flagellates, and to a lesser extent diatoms). This allows ABT larvae to maintain a comparatively low trophic level (~4.2 for preflexion and postflexion larvae) that increases trophic transfer from phytoplankton to larval fish.

INTRODUCTION

The open-ocean Gulf of Mexico (GoM) is a nutrient-poor, lowplankton-biomass region (Biggs and Ressler, 2001; Muller-Karger et al., 2015; Damien et al., 2018; Shropshire et al., 2020). Nevertheless, it is an important region for spawning and larval development of many commercially-important fishes (Lindo-Atichati et al., 2012; Rooker et al., 2012; Rooker et al., 2013; Kitchens and Rooker, 2014; Cornic et al., 2018). The western stock of Atlantic Bluefin Tuna (ABT) travels long distances from feeding grounds throughout the North Atlantic to spawning grounds in the oligotrophic GoM, implying that some characteristics of this region enhance larval success (Rooker et al., 2007; Teo et al., 2007; Rodríguez-Ezpeleta et al., 2019). One strong possibility is that low abundances of potential predators on eggs and larvae and reduced competition for prey in this food-poor region are a prerequisite for pelagic larvae to survive to maturity (Biggs, 1992; Muhling et al., 2017; Laiz-Carrión et al., 2019; Shropshire et al., this issue), but also local enrichment processes such as fronts and eddies may provide areas of higher productivity (Bakun, 2006) increasing chances of larval survival (Bakun and Broad, 2003; Ciannelli et al., 2015). ABT larvae

could then exploit available food resources which can transfer biomass originated from microbial loops to tuna larvae, despite low mean primary productivity. Nevertheless, it remains unclear how ABT and other GoM larval fishes manage to obtain sufficient nutrition during their critical first-feeding period. Discerning the structure of GoM planktonic food webs is crucial to answering such questions.

ABT larvae are selective feeders that rely disproportionately on specific prey taxa including calanoid and poecilostomatoid copepods, cladocerans, and appendicularians (Llopiz et al., 2010; Llopiz et al., 2015; Tilley et al., 2016; Uriarte et al., 2019; Shiroza et al., this issue). These prey items, however, have distinctly different trophic and ecological roles (Landry et al., 2019). Appendicularians are filter-feeding pelagic tunicates with fine meshes that give them access to some of the smallest cyanobacteria in the ocean (Alldredge, 1976; Gorsky and Fenaux, 1998). Poecilostomatoid copepods, by contrast, are predators of other metazoan zooplankton, and hence likely feed comparatively high on the food chain (Turner, 1986). Cladocerans and calanoid copepods are often omnivorous filter feeders, although calanoid copepods can fill multiple trophic roles within the planktonic food web, including as predators on other metazoans (Uye and Kayano, 1994; Mauchline, 1998; Katechakis and Stibor, 2004; Bode et al., 2015).

Elucidating the linkages between larval fish, their prey, and the base of the planktonic food web is crucial to predicting climate change impacts on larval survival (Landry et al., 2019). Different phytoplankton groups (e.g., Prochlorococcus, Trichodesmium, diatoms, mixotrophic nanoflagellates) will respond differently to warming, acidification, and increased stratification in the oligotrophic ocean (Rost et al., 2008; Flombaum et al., 2013; Flynn et al., 2013; Barton et al., 2016; Hong et These variable responses originate from different physiological responses to stressors, but also to fundamentally different relationships between these groups and limiting nutrient, light, or temperature conditions. For instance: Trichodesmium and other diazotrophs (N2-fixing phytoplankton) are not nitrogen limited, Prochlorococcus is adapted to utilizing recycled nitrogen available at low concentrations in oligotrophic regions, and nanoflagellates may rely partially on phagotrophic behavior (mixotrophy) to alleviate nutrient stress (Scanlan and Post, 2008; Zehr, 2011; Stoecker et al., 2017). The pathways that connect different nutrient sources (upwelling, lateral advection, recycled production, and diazotrophy) through phytoplankton and zooplankton to larval fishes will determine how these organisms respond to climate change.

Here, we use linear inverse ecosystem models (LIEM) as a data synthesis tool to constrain pelagic food webs of the oligotrophic GoM. We utilize results from field experiments designed to investigate the open-ocean GoM ecosystem from nutrients to fish (Gerard *et al.*, this issue). LIEM allows us to incorporate diverse ecosystem measurements (e.g., primary productivity, protistan grazing rates, copepod δ^{15} N, and larval ABT gut contents) into a mass-balance-constrained ecosystem model. We use the results to address four distinct questions: What is the trophic level of larval ABT? What is the trophic efficiency of food chains leading to larval ABT? Which phytoplankton groups ultimately support secondary production by larval ABT? What nitrogen sources support the specific food web pathways utilized by larval ABT?

METHODS

In situ measurements

Our data are derived from two cruises in ABT spawning grounds in April-May 2017 and 2018 as part of the Bluefin Larvae in Oligotrophic Ocean Foodwebs: Investigating Nutrients to Zooplankton in the Gulf of Mexico (BLOOFINZ-GoM) Project (Table 1). During these cruises, we conducted regional zooplankton sampling surveys, guided partly by the Bluefin Tuna Index (Domingues *et al.*, 2016), to identify contrasting open-ocean water parcels with and without high abundances of ABT larvae (Gerard *et al.*, this issue). We then conducted three- to five-day Lagrangian experiments (hereafter "cycles"), while following satellite-enabled drift arrays with 3×1-m holey-sock drogues centered at 15 m depth that allowed us to follow patches of mixed-layer water (Landry *et al.*, 2009; Stukel *et al.*, 2015). Five experimental cycles were conducted; in this study, however, we focus only on two experimental cycles with high larval ABT abundance -- hereafter, Cycle 1 (C1) from the 2017 cruise and C5 from the 2018 cruise.

During each cycle, we conducted daily profiles with a CTD-Niskin rosette to measure temperature, salinity, and density and collect samples for chlorophyll a measurements (acidification method, Strickland and Parsons, 1972), phytoplankton pigment analyses (high-pressure liquid chromatography), picophytoplankton and heterotrophic bacteria enumeration (by flow cytometry; Selph $et\ al.$, 2016; Selph $et\ al.$, this issue), nano- and microphytoplankton biomass (Taylor and Landry, 2018; Selph $et\ al.$, this issue), Trichodemium biomass (Selph $et\ al.$, this issue), nutrients (nitrate and ammonium; Knapp $et\ al.$, this issue), dissolved organic nitrogen (DON, Knapp $et\ al.$, this issue), particulate organic nitrogen (PON, Stukel $et\ al.$, this issue), and δ^{15} N of nitrate, DON, and PON (Knapp $et\ al.$, this issue); Stukel $et\ al.$, this issue).

We also conducted a suite of daily *in situ* rate measurements that were incubated in mesh bags affixed at 6 depths spanning the euphotic zone on one of the floating arrays. These measurements included nitrate uptake (Yingling *et al.*, this issue), net primary production (Yingling *et al.*, this issue), and group-specific phytoplankton growth and mortality due to protistan grazing (Landry *et al.*, 2016; Landry *et al.*, this issue). All *in situ* incubations were conducted for 24 h at natural light and temperature conditions. We also conducted shorter (4-6 h) shipboard incubations for nitrate and ammonium uptake (Yingling *et al.*, this issue).

Twice per day (mid-day and midnight) we conducted oblique net tows through the euphotic zone to collect mesozooplankton that were analyzed for carbon, nitrogen, isotopes and gut pigment content (Landry and Swalethorp, this issue). Gut pigment contents were analyzed as in Décima *et al.* (2016) to estimate grazing rates (Landry and Swalethorp, this issue). ABT larvae were sampled frequently by standard double oblique tows (~8 tows d-1) with a 90-cm square bongo net (500-µm mesh) mounted with flowmeters to a depth of 25 m to ensure that we remained inside ABT habitat. Individual tuna larvae (2,055 larvae, ranging from 3–9 mm length) were sorted onboard and identified ABT were liquid nitrogen or ethanol preserved for further analysis of abundance, body size, dry weight, gut content, otolith-based age, and isotopic

measurements (Laiz-Carrion et al., 2015; García et al., 2017; Malca et al., 2017; Laiz-Carrión et al., 2019; Malca et al., in prep.; Shiroza et al., this issue).

Nitrogen inputs to and outputs from the euphotic zone were constrained using sediment traps, Thorpe-scale analyses, and remotesensing products of lateral PON transport. Surface-tethered drifting sediment traps were used to collect sinking PON, chlorophyll, and phaeopigments at 50 m depth, near the base of the euphotic zone (~120 m), and beneath the euphotic zone (200 m) (Stukel et al., this issue). We used Thorpe-scale analyses and nitrate concentration profiles to constrain vertical eddy diffusivity and upward nitrate flux (Gargett and Garner, 2008; Kelly et al., in review). We combined day-night differences in mesozooplankton biomass with allometric ammonium-excretion relationships to quantify active transport by diel vertical migrants (Ikeda, 1985; Landry and Swalethorp, this issue). We also quantified lateral transport of organic matter into the oligotrophic GoM using two independent approaches: combination of remote-sensing-derived estimates of currents with remote-sensing-derived particulate carbon and a biogeochemical model developed for the open-ocean GoM (Shropshire et al., 2020; Kelly et al., in review).

Food web structure

Our food web structure was specifically designed to address the variability in trophic pathways within GoM foodwebs that channel energy towards the prey of ABT larvae (either efficiently or inefficiently) or to the multiple plankton taxa that are not suitable prey for ABT larvae (Fig. 1). The model includes three inorganic N classes (NO₃-, NH₄+, and N₂) and three non-living organic matter pools (DOM, small detritus, and large detritus). It includes four phytoplankton: Trichodesmium, picophytoplankton (assumed to be potentially diazotrophic), diatoms, and mixotrophic flagellates. It also includes heterotrophic bacteria, heterotrophic nanoflagellates, and microzooplankton. Six suspensionfeeding mesozooplankton are included: appendicularians (the only suspension feeders capable of feeding on cyanobacteria and heterotrophic bacteria), vertically-migrating calanoid copepods, non-verticallymigrating calanoid copepods, cladocerans, other non-verticallymigrating herbivorous suspension feeders, and other vertically-migrating herbivorous suspension feeders. It includes two small predatory mesozooplankton: chaetognaths and poecilostomatoid copepods. It also includes 4 "higher trophic levels" that serve as closure terms in the model: preflexion ABT larvae, postflexion ABT larvae, other planktivorous fish, and predatory gelatinous zooplankton (e.g., ctenophores and cnidarians). ABT are assumed to feed on microzooplankton, appendicularians, cladocerans, non-verticallymigrating calanoid copepods, and poecilostomatoid copepods. Piscivory is not included in the model, because field results showed that ichthyoplankton are not important prey to the 3–9 mm larvae (Shiroza et al., this issue). However, piscivory should be added if the model is used for larger larvae or in regions with higher ichthyoplankton densities. Other trophic pathways are determined based on known predator-prey relationships. Because ABT larvae feed only in the mixed layer, we include two layers in the model: upper euphotic zone (0-50 m) and deep euphotic zone (50-100 m on C1; 50-85 m on C5). All model compartments are identical, except that ABT larvae only exist in the upper euphotic zone. The two layers are connected through upward flux of nitrate, downward flux of sinking particles and the motions of verticalmigratory taxa, which are assumed to freely migrate into and between the two layers during the night, but reside beneath the euphotic zone (i.e., outside the model) during the day. Inputs to the model include upwelled

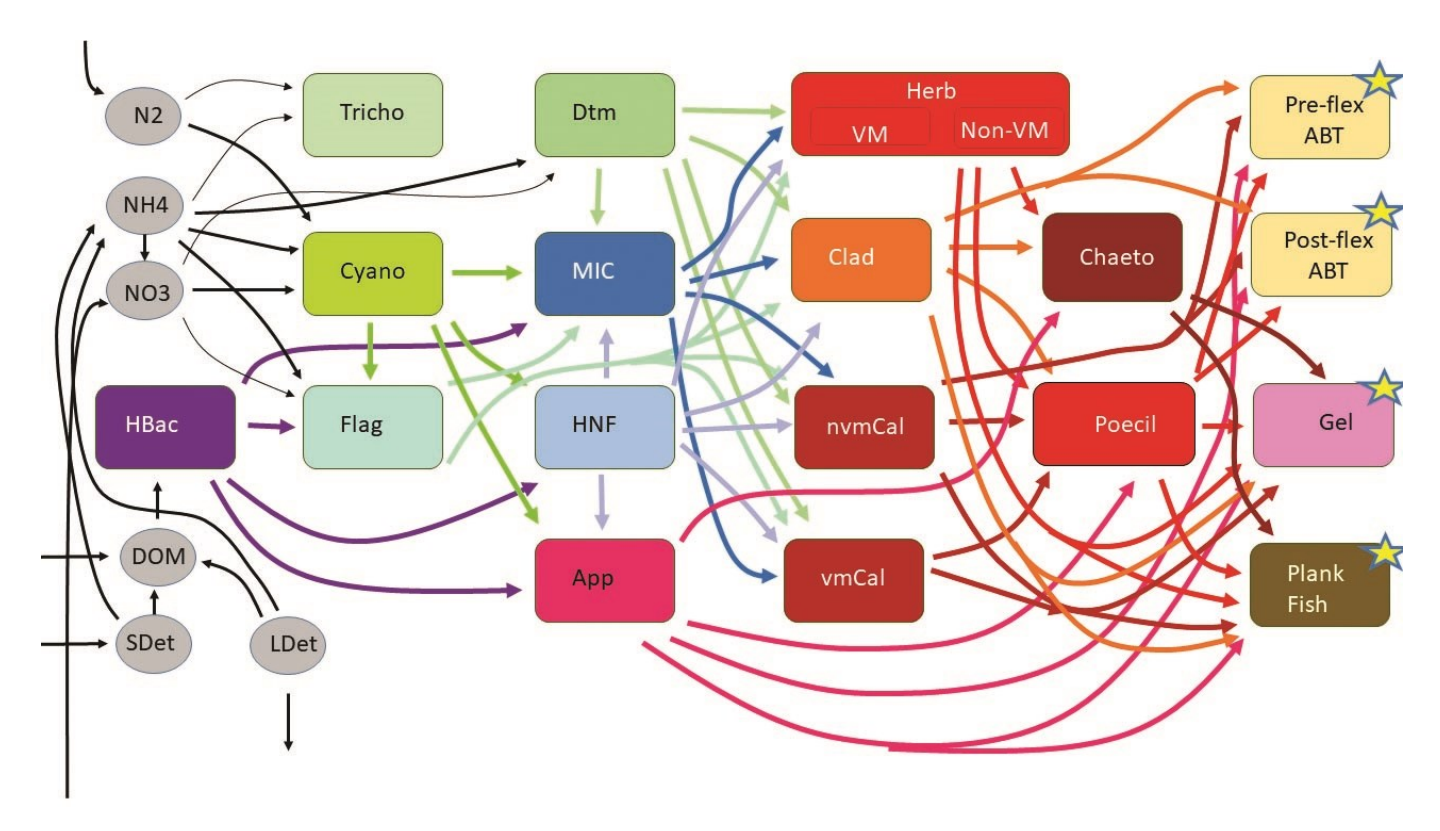


Fig. 1 – Food web structure. All major food web flows between living organism groups are shown. However, for visual simplicity, we omit production of NH₄⁺, DOM, and detritus by all living groups as well as consumption of detritus by protistan zooplankton and suspension-feeding metazoans. Stars indicate groups at the highest trophic levels, for which secondary production is a model closure term. The model has a two-layer structure (~mixed layer and deep euphotic zone) with all trophic components in both layers, except for larval ABT. For all model flows, see Supp. Table 1. HBac = heterotrophic bacteria; DOM = dissolved organic matter; SDet = small detritus; LDet = large (sinking) detritus; Tricho = Trichodesmium; Cyano = cyanobacteria; Flag = mixotrophic flagellates; Dtm = diatoms; MIC = microzooplankton; HNF = heterotrophic nanoflagellates; App = appendicularians; HerbVM = vertically-migrating herbivorous suspension feeders; HerbNVM = non-vertically migrating calanoid copepods; VmCal = vertically-migrating calanoid copepods; Chaeto = chaetognaths; Poecil = poecilostomatoid copepods; Preflex ABT = preflexion Atlantic Bluefin tuna; Postflex ABT = postflexion Atlantic Bluefin tuna; Gel = gelatinous predators (ctenophores and cnidarians); PlankFish = planktivorous fish.

nitrate, diazotrophy, and lateral advection of POM and DOM. Closure terms include secondary production of higher trophic levels, sinking of large detritus, sinking of diatoms, sinking of mixotrophic flagellates, and excretion from vertical migratory taxa beneath the euphotic zone. We assume Redfield stoichiometry for all model flows, which allows us to relate respiration to ammonium excretion. We thus use the term "respiration" when relating respiratory or excretory fluxes to primary production and the term "excretion" when discussing nutrient recycling. Supp. Table. 1 shows all model flows.

Inverse model solution

To constrain the flux of nitrogen through unmeasured ecosystem pathways, we used LIEM techniques (Vézina and Platt, 1988; van Oevelen *et al.*, 2010) to specify mass-balance constraints that must be exactly fit by food-web solutions, approximate equations that quantify measured rates with associated measurement uncertainty, and inequality constraints that represent *a priori* acceptable ranges for different ecosystem properties (e.g., gross growth efficiency varies from 10-40%). We used a total of 44 mass-balance constraints, 80 approximate equalities, and 533 inequality constraints. However, with 302 total unknown food-web flows, the system remains under-constrained. To objectively determine representative solutions (and confidence limits) for all flows, we used the Markov Chain Monte Carlo (MCMC) with ¹⁵N

approach (Stukel *et al.*, 2018a; Stukel *et al.*, 2018b). The MCMC approach conducts a random walk through the solution space constrained to fit the exact equations and bounded by the inequality constraints (Kones *et al.*, 2009; Soetaert *et al.*, 2009; Van den Meersche *et al.*, 2009). New solutions are accepted based on the relative misfits of the new and previous solutions with respect to the approximate equality measurements. The mean solution of the MCMC approach has been shown to more accurately recover withheld measurement constraints than the previously used L₂ minimum norm approach (Stukel *et al.*, 2012; Saint-Béat *et al.*, 2013). The MCMC+¹⁵N approach used herein allows for the incorporation of non-linear constraints associated with unknown δ¹⁵N values for some organisms or non-living nitrogen pools in the ecosystem to further constrain the system. For additional details, see the online supplementary appendix.

Food web analyses

Trophic levels (TL) for all zooplankton were computed as one plus the ingestion-weighted mean TL of prey ($TL_{consumer} = \sum (TL_{prey,i} \times F_{prey,i \to consumer})/\sum F_{prey,i \to consumer}$, where $TL_{prey,i}$ is the trophic level of prey i and $F_{prey,i \to consumer}$ is the rate of feeding of the consumer on prey i). All phytoplankton were assumed TL=1, except mixotrophic flagellates, which had $TL = (1 - p_{phag}) + p_{phag}(1 + p_{phag})$

 TL_{prey}), where p_{phag} is the proportion of their nitrogen derived from phagotrophy (rather than dissolved nutrient uptake). Heterotrophic bacteria were assumed to have a TL equal to one plus the TL of the organism producing the organic matter they utilized.

To quantify indirect nitrogen flows through the food web, we used indirect food web flow analysis (Hannon, 1973). The normalized amount of nitrogen (direct and indirect) that any organism derives from any other organism (or non-living nitrogen pool) can be computed as $(I-G)^{-1}$, where I is the identity matrix and G is the normalized production matrix (i.e., a matrix giving the percentage of an organism's nitrogen requirement derived from any other organism).

Following Stukel *et al.* (2012), we defined three major food web pathways that describe energy and nutrient fluxes from the base of the food web: the herbivorous food chain, the multivorous food chain, and the microbial loop. i) The herbivorous food chain = the sum of direct nitrogen flux from phytoplankton to metazoan zooplankton. ii) The multivorous food chain = the sum of nitrogen flux that reaches metazoan zooplankton after passing through protistan grazers. iii) The microbial loop = the sum of bacterial respiration and the fraction of protistan respiration that was supported by bacterial production. Results for each parameter are presented as means and 95% confidence intervals.

RESULTS

Model performance

The LIEM demonstrates close agreement with field measurements. The square root mean squared error, which can be thought of as the average number of standard errors that model estimates were from the measurements, was 1.17 for C1 if we consider only the field rate measurements and 1.53 for all approximate equality equations (including the $\delta^{15}N$ mass balance equations). For C5 the equivalent values were 1.40 and 1.65. One of the largest model-data mismatches was for sinking flux from the shallow to the deep euphotic zone during C1. The model struggled to find solutions that matched observations showing three-fold higher sinking nitrogen flux from the upper euphotic zone to the lower euphotic zone than out of the euphotic zone. The model also slightly overestimated grazing of suspension-feeding zooplankton on phytoplankton during both cycles, although in this case the model's 95% confidence intervals overlapped the measured values. The model accurately recovered ingestion rates of larval ABT on most mesozooplankton groups (Fig. 2b). The greatest model-data mismatch associated with larval ABT was for feeding on microzooplankton during C5 and by feeding on poecilostomatoid copepods by preflexion larvae during both cycles. In all of these cases, none of the dietary items were found in the guts of the respective field-collected larvae (Shiroza et al., this issue), while the model was constrained to take on positive values for all possible food-web fluxes. Model solutions were also strongly constrained by the comparatively low $\delta^{15}N$ of larval ABT (Table 1). The model struggled to determine solution vectors that matched the comparatively low $\delta^{15}N$ of larval ABT with the fairly similar measured δ15N of upwelled nitrate, sinking detritus, and bulk suspended organic matter, thus leading to model misfits in the $\delta^{15}N$ mass balance equations.

Food web dynamics

Food web dynamics broadly reflected those expected for an oligotrophic, recycling-dominant ecosystem. NH₄⁺ was the dominant source of nitrogen to phytoplankton in the shallow euphotic zone (mean = 84%; 95% C.I. = 70-94% for C1 and 83%; 73-93% for C5). NO₃-uptake (13%, 4-25% for C1; 16%, 6-25% for C5) and N₂ fixation (1.2%, 0.03-4.3% for C1; 1.2%, 0.03-4% for C5%) were comparatively less important. Nutrient utilization patterns were broadly similar in the vicinity of the deep chlorophyll maximum (>50 m depth), although they varied between the two cycles with nitrate becoming substantially more important in the deep euphotic zone during C1 (42%, 13-72% for C1)

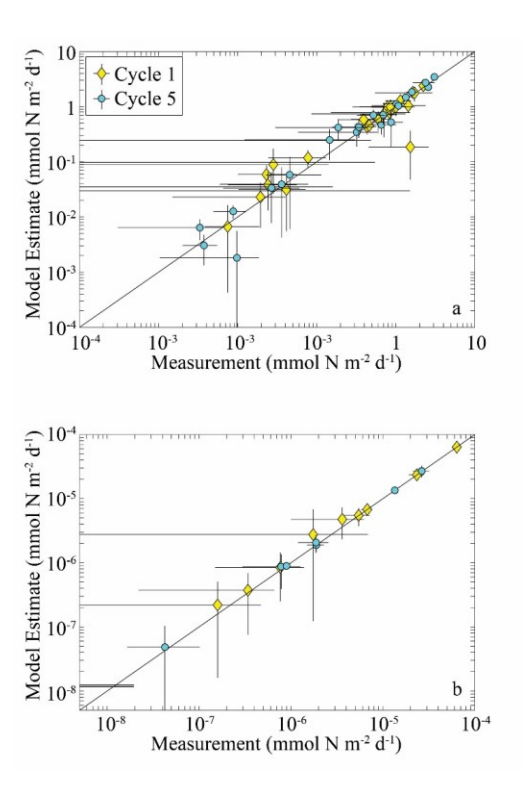


Fig. 2 – Comparison between field measurements and model estimates for planktonic ecosystem rates (a) and ABT feeding measurements (b).

than during C5 (10%, 4-17% for C5). Total production was slightly higher in the shallow euphotic zone (2.4 mmol N m $^{-2}$ d $^{-1}$, 2.2-2.6 mmol N m $^{-2}$ d $^{-1}$ for C1; 3.5, 3.2-3.7 mmol N m $^{-2}$ d $^{-1}$ for C5) than in the deep euphotic zone (1.8 mmol N m $^{-2}$ d $^{-1}$, 1.7-1.9 mmol N m $^{-2}$ d $^{-1}$ for C1; 1.5, 1.4-1.6 mmol N m $^{-2}$ d $^{-1}$ for C5).

Most primary production was from picophytoplankton (54%, 40%-68% for C1; 79%, 68-90% for C5) and flagellates (42%, 28-55% for C1; 21%, 14-28% for C5) in the shallow euphotic zone, as suggested by the field data. Diatoms were comparatively less important (4.9%, 3.2-6.8% for C1; 0.4%, 0.3-0.5% for C5), while *Trichodesmium* production was negligible. The relative proportions of each group were fairly similar at the deep chlorophyll maximum. Mixotrophic flagellates derived 18% (C1) and 24% (C5) of their nitrogen from phagotrophy in the shallow euphotic zone (and slightly more in the deep euphotic zone). They consumed more heterotrophic bacteria than cyanobacteria.

Phytoplankton mortality was dominated by protistan grazing. These zooplankton (including mixotrophic flagellates) consumed 64% (49-79%) of phytoplankton production during C1 and 54% (47-61%) during C5. Metazoan zooplankton consumed a lower portion of phytoplankton production (20%, 14-26% for C1; 23%, 16-30% for C5), although they consumed more of the production of diatoms than protists did. Suspension-feeding metazoans also relied heavily on protistan zooplankton as dietary sources. This was reflected in trophic positions that averaged greater than 3.0 for all metazoans except appendicularians (Fig. 3a-d). In the upper euphotic zone predatory zooplankton (poecilostomatoid copepods, chaetognaths, and gelatinous predators) had particularly high trophic positions of 4.4, 4.4, and 4.7, respectively, for C1 (Fig. 3a) and 4.3, 4.3, and 4.6 for C5 (Fig. 3c). Their mean trophic positions in the deep euphotic zone were similar (4.3, 4.3, and 4.6 for C1 (Fig. 3b) and 4.1, 4.1, and 4.4 for C5 (Fig 3d) for poecilostomatoid copepods, chaetognaths, and gelatinous predators, respectively).

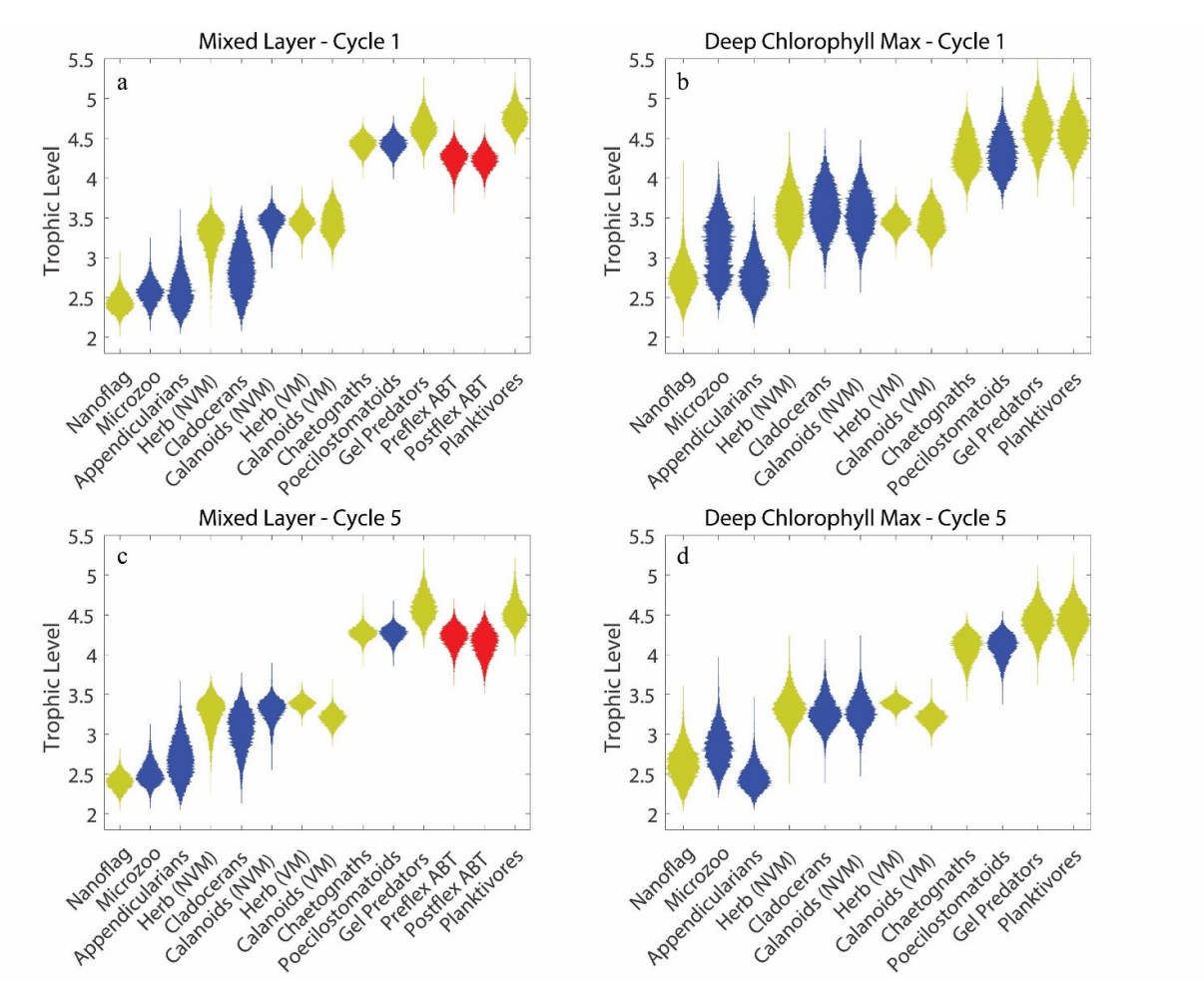


Fig. 3 – Violin plots of trophic level of zooplankton and fish in the mixed layer (a, c) and deep chl max (b,d) during C1 (a,b) and C5 (c,d). Blue plots are ABT prey. Red plots are ABT.

Quantification of major food web pathways showed that the GoM euphotic zone is dominated by the microbial loop (Fig. 4). The microbial loop (defined as respiration by heterotrophic bacteria and the proportion of protistan respiration supported by bacterial production) processed 70% (51-90%) of net primary production in the shallow euphotic zone (Fig 4a) and 77% (61-91%) of net primary production in the deep euphotic zone (Fig. 4b) during C1, whereas during C5 it used 71%; 58-84% in the upper euphotic zone (Fig. 4c) and 81%; 65-96% in the lower euphotic zone (Fig. 4d). For comparison, the herbivorous and multivorous food chains were responsible for processing 7.2% and 46% of net primary production (NPP), respectively, in the shallow euphotic zone (Fig. 4a) and 37% and 46%, respectively in the deep euphotic zone (Fig. 4b) during C1. During C5 the herbivorous and multivorous food chains were responsible for 9.8% and 70% of NPP in the shallow euphotic zone (Fig. 4c) and 54% and 44% in the deep euphotic (Fig. 4d). The dominance of microbial loop pathways aligns with the importance of recycled NH₄⁺ for phytoplankton production and conforms with an expectation of tight recycling in oligotrophic ecosystems with limited new nutrient supply. In the shallow euphotic zone, where recycling and the microbial loop were most important, DON production was substantial (2.0 and 2.9 mmol N m⁻² d⁻¹, for C1 and C5). Phytoplankton and protistan zooplankton had

large roles in DON production (38% and 32%, respectively) during C1, with the remainder primarily coming from dissolution of detritus (9.8%) and mesozooplankton excretion (11%). During C5, phytoplankton exudation was responsible for 47% of DON production, while protists were responsible for 28% and metazoan zooplankton contributed 15% of DON production. Bacterial excretion was in turn responsible for 50% of NH₄ $^+$ regeneration in the shallow euphotic zone during C1 and 46% during C5, with protist excretion generating an additional 32% (C1) or 29% (C5), and mesozooplankton excretion producing 15% (C1) or 20% (C5) of the NH₄ $^+$ used by phytoplankton.

Larval Atlantic Bluefin Tuna in the GoM Ecosystem

As suggested by the gut content data, model results show that larval ABT feed predominantly on cladocerans and calanoid copepods, with a lesser role for microzooplankton, appendicularians, and poecilostomatoid copepods in their diets (Fig. 5). Calanoid copepods comprised 76% of the diet of preflexion ABT (95% C.I. = 59-88%) during C1 and 69% (55-83%) during C5. Microzooplankton (6%; C.I. = 1-13% during C1; 0.4%, 0.03-0.9% during C5), appendicularians (14%; 4-26% during C1; 1.6%, 0.2-3.7% during C5), and cladocerans (4%; 0.3-9% during C1; 29%, 14-42% during C5) were smaller contributors to the diets of preflexion ABT, while poecilostomatoid copepods were

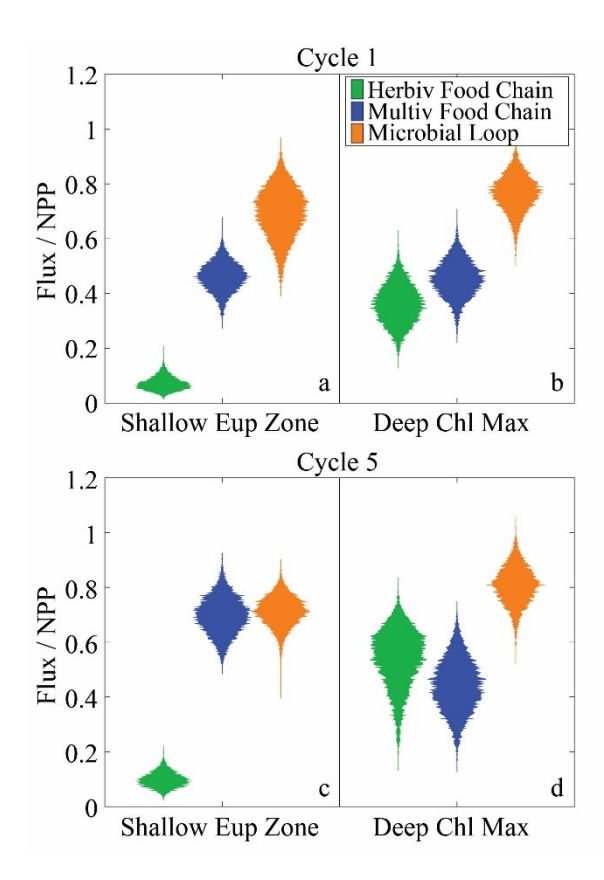


Fig. 4 – Violin plots of nitrogen flux through the herbivorous food chain (phytoplankton to metazooplankton), multivorous food chain (phytoplankton to metazooplankton via protistan grazers), and microbial loop (respiration from bacteria and protists supported by bacterial production) normalized to net primary production for the shallow euphotic zone during C1 (a), deep euphotic zone during C1 (b), shallow euphotic zone during C5 (c), and deep euphotic zone during C5 (d).

negligible contributors to preflexion ABT diets (<0.7% during both cycles) (see Figs. 5a, c). Although calanoid copepods were also the dominant dietary source for postflexion ABT during C1 (62%; 59-66%), these larger larvae also relied substantially on cladocerans (23%; 19-26% during C1; 62%, 57-67% during C5) (see Figs. 5b, d).

The prevalence of suspension-feeding zooplankton in the diets of both preflexion and postflexion diets led to relatively low trophic levels for ABT larvae (Fig. 3a, c). Given the ecosystem structure used in the model (Fig. 1), larval ABT could potentially have a trophic level between 3 and 7. However, both preflexion and postflexion larvae had trophic levels on the low end of this range. Preflexion ABT had a trophic level of 4.2 (4.0-4.5) during C1 and 4.2 (3.9-4.5) during C5, while postflexion ABT had trophic level estimates of 4.2 (4.0 -4.5) during C1 and 4.1 (3.8-4.5) during C5. Both developmental stages of ABT larvae thus had trophic positions averaging ~0.6 of their maximum possible trophic level (Fig. 6) and only one trophic position higher than their theoretically lowest possible trophic level within the food web. The trophic positions of larval ABT were thus notably low relative to those if feeding on the longest possible food chains that the model allowed. Based on this metric, their trophic positions were also notably lower than many of the zooplankton and other fish in the model.

The food chains supporting larval ABT were diverse and relied on significant production of picophytoplankton, flagellates, and diatoms

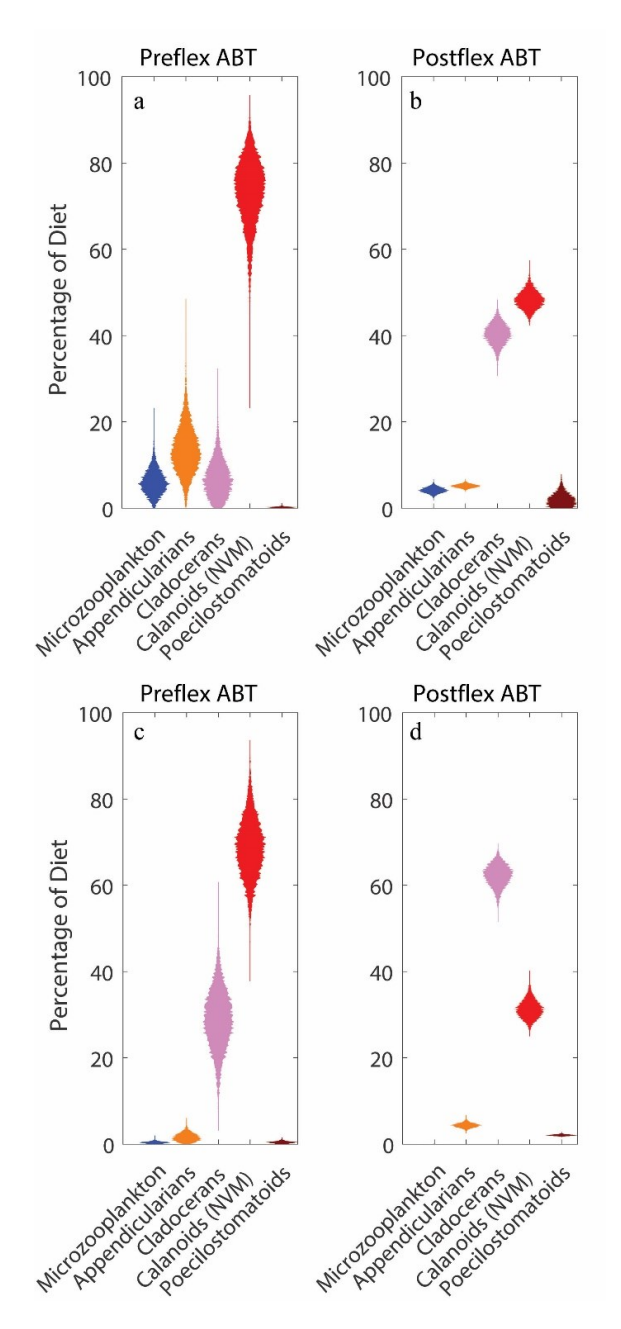
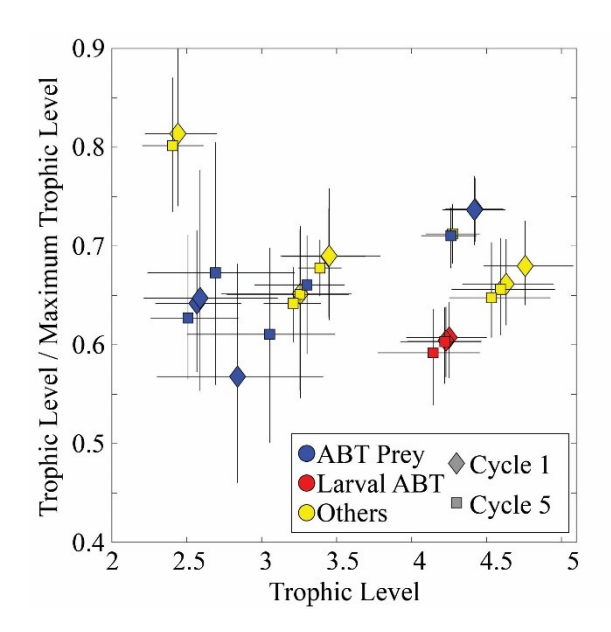


Fig. 5 – Violin plots of modeled larval ABT diets during C1 (a,b) and C5 (c,d).

(while the production of *Trichodesmium* was insignificant for ABT food chains). Preflexion ABT excreted 1.0 (0.4-2.0) nmol N m⁻² d⁻¹ derived from the production of flagellates, 0.9 (0.4-1.8) nmol N m⁻² d⁻¹ from picophytoplankton, and 0.16 (0.05-0.37) nmol N m⁻² d⁻¹ from diatoms during C1 (Fig. 7a). During C5, preflexion ABT excreted 0.37 (0.14-0.79), 0.57 (0.28-0.99) and 0.06 (0.005-0.21) nmol N m⁻² d⁻¹ from flagellates, picophytoplankton, and diatoms, respectively (Fig. 7e). Postflexion larvae excreted 17 (8-29) nmol N m⁻² d⁻¹ from flagellates, 13 (6.7-23) nmol N m⁻² d⁻¹ from picophytoplankton, and 4.1 (1.2-9.2) nmol N m⁻² d⁻¹ from diatoms during C1 (Fig. 7a) and 4.7 (1.8-9.7). 6.7 (3.4-12), and 1.8 (0.14-5.3) nmol N m⁻² d⁻¹ during C5 (Fig. 7e). These values were influenced in large part by the different production rates of each phytoplankton taxa (flagellate, picophytoplankton, and diatom NPP in



 $\begin{array}{ll} \textbf{Fig. 6} - \text{The ratio of the trophic level of different modeled} \\ \textbf{zooplankton and fish to the trophic level they would have in the} \\ \textbf{longest possible model food chain. The "other" category includes} \\ \textbf{all planktivorous fish and all zooplankton that are not larval ABT} \\ \textbf{prev.} \end{array}$

the shallow euphotic zone were 1.8, 1.7, and 0.24 mmol N m⁻² d⁻¹ during C1 and 1.5, 4.2, and 0.015 mmol N m⁻² d⁻¹ during C5). When normalized to phytoplankton NPP, it becomes clear that larval ABT rely disproportionately on the production of large phytoplankton (Fig. 7b, f), even though large phytoplankton production is low in absolute terms. Preflexion ABT respired 1.1×10⁻⁴% (C1) and 4.0×10⁻⁴% (C5) of diatom NPP and 6.3×10^{-5} % (C1) and 2.9×10^{-5} % (C5) of flagellate NPP, compared to only 5.2×10⁻⁵ % (C1) and 1.5×10⁻⁵ % (C5) of picophytoplankton NPP. Postflexion larvae respired 2.9×10⁻³ % (C1) and 1.1×10^{-2} % (C5) of diatom NPP, 1.0×10^{-3} % (C1) and 3.7×10^{-4} % (C5) of flagellate NPP, and 7.5×10^{-4} % (C1) and 1.8×10^{-4} % (C5) of picophytoplankton NPP. The proportion of Trichodesmium NPP respired by larvae was poorly constrained by the model, although Trichodesmium production was consistently low in all model solution vectors. The disproportionately large role of diatoms in larval ABT diets was reflected in the roles of diatoms in supporting their mesozooplankton prey (Fig. 7d, h). Three of the four mesozooplankton prey taxa respired a higher proportion of diatom NPP than any other phytoplankton, while calanoids relied slightly more on flagellates than on diatoms during C5 (although they also preferentially relied on diatoms during C1). These results for mesozooplankton were in stark contrast to similar proportional roles for phytoplankton in protists (Fig. 7c, g). Heterotrophic nanoflagellates relied disproportionately on picophytoplankton, respiring 19% of picophytoplankton NPP during C1 (14% during C5), while microzooplankton relied disproportionately on the NPP of flagellates (respiring 20% of flagellate NPP during C1 and 11% during C5).

Nitrogen cycle and support of the upper euphotic zone ecosystem

In nitrogen-limited ecosystems, such as the open-ocean GoM, the supply of new nitrogen can control overall ecosystem productivity. Our results suggest that in the upper euphotic zone where ABT larvae feed, the ecosystem is not substantially supported by locally-upwelled nitrate (which supplied $4.4 \times 10^{-5} (2.1 \times 10^{-5} - 8.4 \times 10^{-5})$ mmol N m⁻² d⁻¹ to the upper euphotic zone during C1 and $4.3 \times 10^{-5} (2.3 \times 10^{-5} - 8.4 \times 10^{-5})$ mmol N m⁻² d⁻¹ during C5) or by nitrogen fixation (which supplied $0.092 (4.3 \times 10^{-3} - 8.4 \times 10^{-3})$

0.32) mmol N m⁻² d⁻¹ to the upper euphotic zone during C1 and 0.06 (0.002-0.2%) mmol N m⁻² d⁻¹ during C5). Rather, nitrogen entered the ecosystem primarily through lateral advection of organic matter (PON lateral advection = 0.18 mmol N m⁻² d⁻¹, 0.007-0.51 mmol N m⁻² d⁻¹ during C1; 0.94 mmol N m⁻² d⁻¹, 0.30-1.6 mmol N m⁻² d⁻¹ during C5; DON lateral advection = 0.19 mmol N m⁻² d⁻¹, 0.007-0.45 mmol N m⁻² d⁻¹ during C1; 0.10 mmol N m⁻² d⁻¹, 0.002-0.37 mmol N m⁻² d⁻¹ during C5) from more productive regions (likely from shelf-break regions in the northern GoM, Gerard *et al.*, this issue). Indeed, ABT derived only 0.2% (0.004-0.7%) of their nitrogen from upwelled nitrate during C1 and 0.1% (0.003-0.46%) during C5 and 2.2% (0.2-7.6%) and 0.95% (0.08-3.3%) of their nitrogen from nitrogen fixation during C1 and C5, respectively. They derived 98% (92- >99%) and 99% (97- >99%) from lateral advection.

This laterally-advected organic matter entered the planktonic food web through multiple pathways. DON was utilized by bacteria, which had a gross growth efficiency of 27% (20-30%) during C1 and 28% (24-30%) during C5 and hence converted 73% of the DON they utilized to NH₄⁺ during C1 and 72% during C5. The suspended particles that we assume comprised laterally-advected PON were consumed primarily by protistan grazers or were converted into DON (likely through the activity of particle-attached microbes that were not explicitly included in our model). This highlights the importance of the microbial food web in mediating and enhancing phytoplankton in oligotrophic regions. Indeed, even nitrate (which is often considered to be a "new" nutrient in the euphotic zone) was primarily produced in situ by microbial activity (i.e., nitrification conducted by implicitly modeled ammonium-oxidizing bacteria). Modeled nitrification rates in the upper euphotic zone were 0.45 (0.15-0.83) mmol N m⁻² d⁻¹ during C1 and 0.08 (0.3-1.3) mmol N m⁻² d⁻¹ during C5. This equates to nitrification rates of 8.9 and 16 nmol N L⁻¹ d⁻¹ for C1 and C5, respectively. Notably, despite these low absolute nitrification rates, nitrate in the surface ocean was able to be regenerated every 2-3 days, because nitrate concentrations were consistently low in the upper euphotic zone. Considering that ammonium concentrations were ~90 nmol L⁻¹ during C1 and ~50 nmol L⁻¹ during C5, this suggests a specific ammonium-oxidation rate of 0.1 d⁻¹ during C1 and 0.32 d⁻¹ during C5. These results highlight the complexity of microbial and zooplankton linkages that support larval ABT in their oligotrophic nursery regions and suggest that the circulation of the GoM plays an important role in sustaining suitable conditions for larval growth.

DISCUSSION

The open-ocean GoM is an incredibly oligotrophic ecosystem with low productivity and a deep nitracline (Biggs, 1992; Gomez et al., 2018; Knapp et al., this issue; Yingling et al., this issue). Nevertheless, it is an important spawning ground for many migratory fish species, including multiple species of tuna, dolphinfish, sailfish, and marlin (Rooker et al., 2012; Kitchens and Rooker, 2014; Cornic et al., 2018; Laiz-Carrión et al., 2019). It is also a region in which substantially depressed vertical mixing limits phytoplankton productivity during ABT spawning periods (Gomez et al., 2018). If nutrient supply is indeed crucial for supporting these oligotrophic systems, predicted future warming and increased stratification could have deleterious impacts on taxa living in the mixed layer (Muhling et al., 2011; Liu et al., 2015; Muhling et al., 2015). Understanding how pelagic ecosystems and the larval fish they support will respond to climate change requires knowledge of the food web pathways that convert phytoplankton production into the preferred prey of different species (Landry et al., 2019).

We can hypothesize two potential ways in which an organism's diet could make it well adapted to life in an oligotrophic region. First, it could feed preferentially on taxa that have either direct or indirect linkages to some of the most abundant primary producers in the ecosystem (e.g., cyanobacteria). For instance, a reliance on appendicularians would give

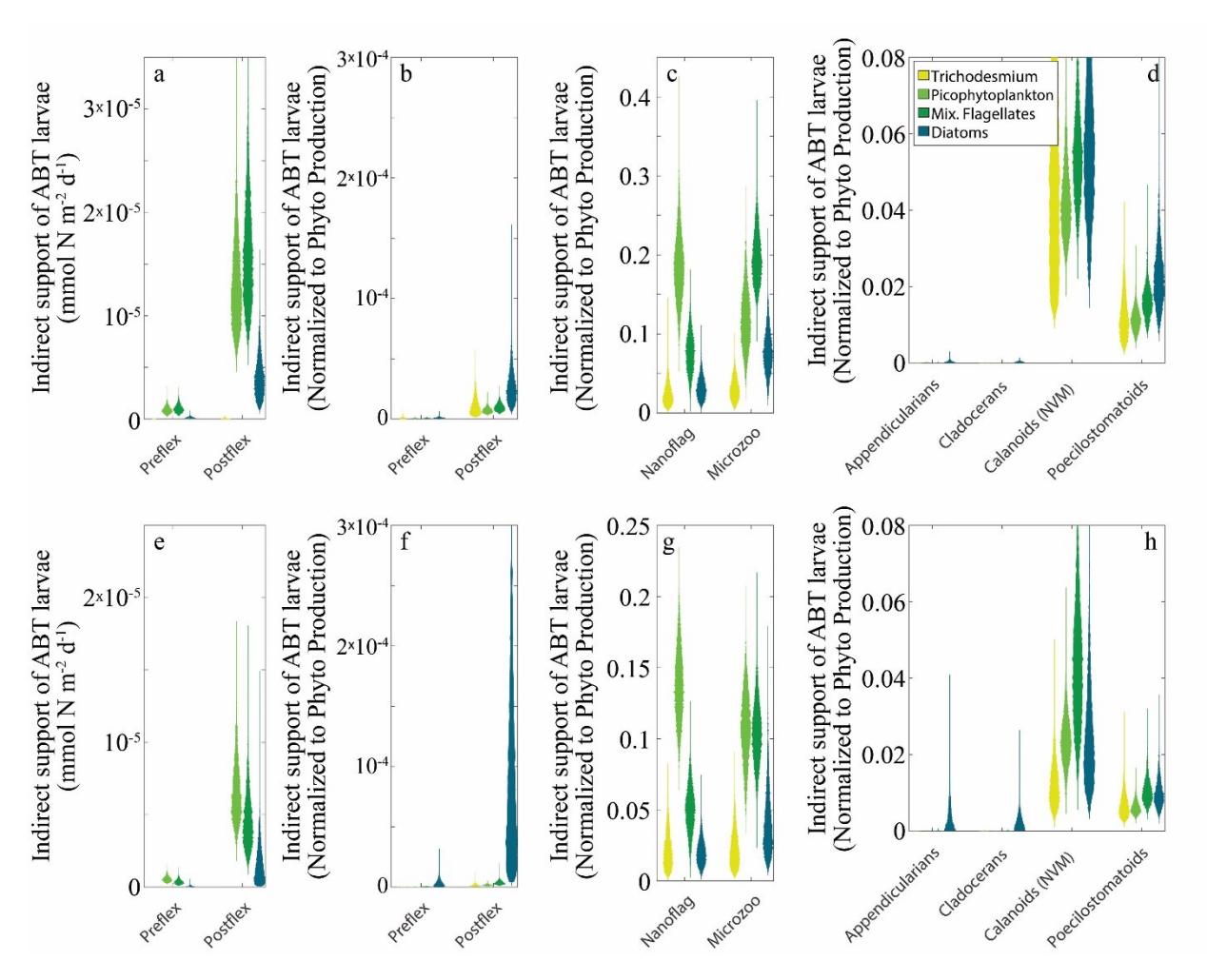


Fig. 7 – Indirect food web flows to larval tuna (a,b,e,f), protists (c,g), and mesozooplankton (d,h). Panels a and e show the amount of organic matter derived from each phytoplankton taxon that was respired by larval tuna. Other panels show the proportion of the production of each phytoplankton taxon that was respired by either larval tuna (b,f), protists (c,g), or mesozooplankton (d,h). Only ABT prey are shown in d and h. Panels a-d are for C1; e-h are for C5.

larval fish access to a suspension feeder that can consume picophytoplankton directly (Gorsky and Fenaux, 1998; Llopiz *et al.*, 2010). Conversely, preference for calanoid copepods and podonid cladocerans would make a larval fish more dependent on the production of diatoms and other large phytoplankton. A second, but not mutually-exclusive, hypothesis is that larval fish are more likely to thrive in oligotrophic ecosystems if they feed at a low trophic position, thus maximizing trophic transfer efficiency from phytoplankton to larvae, regardless of the source of production.

Our results provide no evidence for the former hypothesis. Although diatom production only contributed to ~10% of ABT larval diets, it was a disproportionately high fraction of the ABT diet relative to the proportional role of diatoms to total NPP in the upper euphotic zone (~5% during C1, <1% during C5). Indeed, relative to a phytoplankton taxon's productivity, the proportional contribution of each phytoplankton taxon to food-web pathways that support pre- and postflexion ABT larvae increased with increasing phytoplankter size from picophytoplankton to flagellates to diatoms (Fig. 7). The disproportionately large role of diatom-driven pathways was largely the result of the important role that podonid cladocerans played in ABT diets. Although they were only abundant in the water column during C5, our experiment conducted

closest to the shelf break, podonids were consistently over-represented in ABT guts (Shiroza et al., this issue). Cladocerans are more frequently found in coastal regions of the GoM, suggesting that they prey preferentially on large phytoplankton, as suggested by the LIEM and consistent with feeding studies (Kim et al., 1989; Katechakis and Stibor, Non-vertically-migrating calanoid copepods, which formed another important component of ABT diets (because they were the most abundant mesozooplankton prey available to ABT), had a more diverse diet of diatoms, mixotrophic flagellates, and heterotrophic protists. In contrast, while efficient pathways from cyanobacteria to ABT larvae can occur through appendicularians and microzooplankton, these taxa were not abundant in ABT guts. Appendicularians were rare in the water column, while microzooplankton were abundant but seldom selected by ABT. The majority of cyanobacteria were consumed by heterotrophic nanoflagellates. These heterotrophic nanoflagellates had moderate gross growth efficiency in the model (30-36%) and were preyed upon by other protists (microzooplankton) and suspension-feeding metazoans. Cyanobacteria and heterotrophic nanoflagellates thus contributed disproportionately to the recycling pathways of the microbial loop, forming a largely distinct food web from the multivorous and herbivorous pathways, which mostly began with mixotrophic flagellates and diatoms and supported the production of larval ABT and other planktivorous fish. Despite distinct differences in prey selectivity with ontogeny (large cladocerans were much more important prey for postflexion larvae, Shiroza *et al.*, this issue) our results show similar dependence on large phytoplankton for both larval stages.

Our results offer more support for the hypothesis that ABT larvae feed at a relatively low trophic level, maximizing the proportion of NPP available to them and helps explain how they survive in their oligotrophic spawning grounds (Fig. 6). The trophic position of ABT larvae (~4) is much closer to the minimum trophic level that our model allows (3: phytoplankton → prey → larvae) than to the maximum allowed trophic level (7: phytoplankton → bacteria → nanoflagellates → microzooplankton → suspension-feeders → carnivorous zooplankton → larvae). The low trophic position of ABT larvae is particularly striking considering the relatively weak herbivorous food chain. Generally, planktivorous fish are more likely to be at a low trophic level in an ecosystem classically dominated by large phytoplankton and herbivorous mesozooplankton. However, the herbivorous food chain was responsible for only 7.2% (C1) or 9.8% (C5) of net primary production processing in the shallow euphotic zone where ABT larvae feed; the multivorous food chain processed 46% (C1) or 70% (C5) of NPP, while the microbial loop processed 70-71% of NPP on both cycles (Fig. 4, note that the total exceeds 100% because NPP does not include phytoplankton DON production). The low trophic positions of ABT larvae were primarily due to two factors: 1) although total protistan secondary production was higher than total mesozooplankton secondary production, a comparatively small proportion of this secondary production made its way to larval tuna; most was dissipated as respiration in the microbial loop. Food chains supporting larval ABT were largely distinct from those involving the smallest class of heterotrophic protists. 2) Both size classes of ABT larvae fed preferentially on podonid cladocerans, which feed lower in the food chain than other suspension-feeding taxa. Shiroza et al. (this issue) found the selection for cladocerans to be an active process, further supporting the notion that ABT larvae are highly specialized at maximizing trophic efficiency within their oligotrophic nurseries.

While the trophic position of ~4 is low for a species known to preferentially feed on carnivorous copepods (poecilostomatoids) in a cyanobacteria and microbial loop-driven ecosystem, we note that this is not actually a low trophic level relative to some other mass-balance constrained marine food web models. Many models based on ECOPATH software include only one (or zero) protistan trophic step and a single mesozooplankton group (Arreguin-Sanchez et al., 2004; Walters et al., 2008; Geers et al., 2016). These models constrain zooplankton to trophic levels 2 or 3; hence, the maximum allowed trophic position for planktivores is only 3 or 4. The additional complexity of our modeled ecosystem is a far more realistic depiction of natural food web complexity (Fig. 1). Even so, our model allows only a maximum of two trophic steps within the protistan zooplankton (heterotrophic nanoflagellates and microzooplankton), which is an arbitrary limit given the fluidity of protistan trophic interactions (Boenigk and Arndt, 2002; Pomeroy et al., 2007; Calbet, 2008; Caron et al., 2012; Sherr and Sherr, 2016). Some protists (e.g., pallium-feeding dinoflagellates) routinely feed at a 1:1 predator:prey size ratio, while others (e.g., ciliates) feed closer to a 10:1 predator:prey size ratio (Kiørboe, 2008; Fuchs and Franks, 2010). Some protists may consequently function at a higher trophic position than allowed by our model.

The BLOOFINZ-GoM study offers new insights to the physical dynamics of the GoM that support larval ABT. Kelly *et al.* (in review) analyzed vertical profiles of nitrate and buoyancy frequency from our cruises and concluded that exceedingly low amounts of nitrate were upwelled into the shallow euphotic zone where ABT spawn and their larvae grow. Instead, results from remote-sensing products and a three-dimensional biogeochemical model provide compelling evidence that

most nitrogen for export in the ABT habitat arrives via horizontal advection of organic matter. While our model constrains these inputs to be non-living organic matter (PON and DON), we note that a substantial proportion of this organic matter might be living plankton advected from more productive regions including the shelf-break region of the northern GoM and the Campeche Banks region north of the Yucatan Peninsula. Indeed, Gerard et al. (this issue) backtracked physical flows for the source of waters sampled in C1 and C5 to their origins 2-4 weeks previously along the shelf-slope margin in the northeastern GoM. Stukel et al. (this issue) found that ~20% of particulate organic carbon in the upper euphotic zone was contained in living organisms. Landry and Swalethorp (this issue) further determined that (particularly during C5) predatory zooplankton likely relied on prey advected into our study region from more productive areas. Shropshire et al. (this issue) showed that ABT survival was also dependent on advection of prey from coastal areas and concluded that the most beneficial region for ABT spawning was near the shelf-break where prey are abundant for first-feeding larvae, but where offshore currents can transport larvae that survive the critical period to more oligotrophic regions before predation becomes a substantial source of mortality.

Our results show the importance of extensive recycling pathways for supporting phytoplankton production in this habitat. Despite the very low rates of vertical nitrate input and nitrogen fixation to the upper euphotic zone, sinking carbon flux from the upper euphotic zone was substantial (Stukel et al., this issue). This export, and indeed nearly all production in the upper euphotic zone, was supported by nutrients regenerated from PON through the activity of heterotrophic bacteria and protistan zooplankton. NH₄⁺ was responsible for ~85% of the production of phytoplankton in the upper euphotic zone, as is commonly the case in the mixed layer of oligotrophic, open-ocean regions (McCarthy et al., 1996; Lipschultz, 2001). However, in contrast to simple interpretations of nitrogen utilization, even NO₃ was primarily generated autochthonously in the shallow euphotic zone and did not represent a "new" form of nitrogen. The utility of nitrate as a tracer of "new" production (Eppley and Peterson, 1979) has been extensively debated in the light of evidence of nitrification in shallow waters (Yool et al., 2007). The emerging consensus suggests that ammonium-oxidizing bacteria are not intrinsically light-inhibited (although some taxa may be), but rather they are often outcompeted in the euphotic zone by Prochlorococcus and other low-nutrient specialist phytoplankton (Smith et al., 2014; Wan et al., 2018; Xu et al., 2019). Our results do not contradict this view. Indeed, the LIEM suggests that phytoplankton utilize NH₄⁺ more rapidly than ammonium-oxidizing bacteria. However, the low NO₃concentrations throughout the euphotic zone (Knapp et al., this issue), and exceedingly low NO₃- flux (Kelly et al., in review) allow nitrification to dominate NO₃ supply despite low absolute nitrification rates. Indeed, our estimate of the specific rate of ammonium oxidation necessary to support phytoplankton NO₃- utilization (0.1-0.3 d⁻¹) is near the median value for surface ocean ammonium oxidation in the synthesis of Yool et al. (2007). Notably, Clark et al. (2008) measured ammonium and nitrite oxidation rates in oligotrophic regions of the Atlantic Ocean slightly lower than our LIEM-predicted values, and Bronk et al. (2014) measured substantially higher nitrification rates in offshore regions of the West Florida Shelf. Nitrification rate measurements from other regions have been highly variable, and there is not, as yet, a consensus on the relative importance of shallow nitrification to NO₃ supply in oligotrophic regions (Newell et al., 2013; Clark et al., 2016; Shiozaki et al., 2016).

The importance of laterally-advected organic matter for supporting oligotrophic communities in the GoM offers important insight into the physical characteristics that make the GoM an ideal spawning habitat for ABT. While previous studies have focused on the role of vertical mixing and upwelling, our results show that mixed layer productivity may be more directly tied to horizontal fluxes driven by the high mesoscale

eddies that it sheds are prominent features enhancing circulation (Forristall et al., 1992; Oey et al., 2005; Schmitz et al., 2005). These features have the potential to fundamentally restructure open-ocean ecosystems, with warm-core eddies (including Loop Current Eddies) depressing the nutricline and primary production, while cold-core eddies increase open-ocean upwelling and productivity (Biggs and Müller -Karger, 1994). These altered nutrient supply and phytoplankton regimes lead to substantially higher zooplankton biomass in cold-core eddies (Wells et al., 2017). However, the relative importance of each eddy type, as well as the distinct gradient regions that form on their edges, on larval ABT remains a topic of active debate (Muhling et al., 2010; Domingues et al., 2016). Our results suggest that both eddy types can be important nitrogen sources to the upper euphotic zone, since the high horizontal velocities along the eddy can transport living and non-living organic matter from high biomass regions to oligotrophic areas, especially when eddies impinge on coastal regions. Shropshire et al. (2020) also found substantial transport into our study region mediated by entrainment of plankton-rich waters from the Campeche Bank into the edges of the Loop Current. Notably, the larvae distribution in the major recognized ABT eastern stock spawning area, around the Balearic Islands in the western Mediterranean basin, is influenced by frontal zones resulting from the convergence of recent and resident Atlantic surface waters (Alemany et al., 2010; Muhling et al., 2017; Reglero et al., 2017). Such mesoscale features have been hypothesized to act as retention larval feeding areas, enhancing particle food concentrations and increasing the probability of survival of larvae that rely substantially on copepodites and cladoceran prey during preflexion stage in this oligotrophic environment (Catalán et al., 2011; Uriarte et al., 2019). Horizontal flows associated with these features may also connect the nearby coastal region to oligotrophic nursery areas, a possibility that should be explored in future studies.

The potential importance of cross-shore fluxes to survival of first-

energy of the GoM. In the oligotrophic GoM, the Loop Current and the

The potential importance of cross-shore fluxes to survival of first-feeding ABT suggests that determining the responses of pelagic food webs and ABT larvae to climate change will require characterizing changes in GoM circulation in response to future forcing, along with the expected food web processes that regenerate nutrients and promote growth of larval ABT prey (Muhling *et al.*, 2011; Liu *et al.*, 2015). Our study offers insight into the processes allowing larval ABT to survive in a food-scare environment. However, substantial additional research is needed to quantify the impacts of spatial and interannual variability, as well as secular change, on these ecosystems and threatened species.

CONCLUSIONS

ABT larvae develop in oligotrophic ecosystems, dominated by cyanobacteria and other small phytoplankton. The major trophic pathway through the microbial loop is highly inefficient, with most production lost to remineralized nutrients by bacteria and multi-step protistan grazing chains. Both pre- and postflexion larval ABT feed preferentially on less dominant pathways associated with herbivorous and multivorous food chains, without pronounced ontogenetic differences in food-web roles between pre- and postflexion stages, despite distinct changes in diet. Consequently, ABT larvae depend on the production of diatoms and mixotrophic flagellates that support herbivorous zooplankton, particularly calanoid copepods and cladocerans. Preferential utilization of these more direct trophic pathways allows the larvae to feed at relatively low trophic levels despite the fact that the taxa responsible for the majority of secondary production in the food web (bacteria and heterotrophic nanoflagellates) are not accessible to them as prey. Further research is needed to understand how these ecological interactions might be altered under different disturbance regimes.

We thank our numerous colleagues in the BLOOFINZ-GoM project who made this research possible.

FUNDING

Our work was funded by National Science Foundation Biological Oceanography grant #1851347 and a National Oceanic and Atmospheric Administration's RESTORE Program Grant (Project Title: Effects of nitrogen sources and plankton food-web dynamics on habitat quality for the larvae of Atlantic bluefin tuna in the Gulf of Mexico) under federal funding opportunity NOAA-NOS-NCCOS-2017-2004875, including NOAA JIMAR Cooperative Agreement, award #NA16NMF4320058, NOAA CIMAS Cooperative Agreement, award #NA15OAR4320064, and NOAA CIMEAS Cooperative Agreement, award #NA15OAR4320071.

https://restoreactscienceprogram.noaa.gov/funded-projects/bluefin-tuna-larvae. We also thank the ECOLATUN (CTM-2015-68473-R MINECO/FEDER) project.

DATA AVAILABILITY

Data utilized in this manuscript are available on NCCOS and BCO-DMO (https://www.bco-dmo.org/project/819488). MCMC+¹⁵N model code is available on Github: https://github.com/stukel-lab. The specific code used to run the BLOOFINZ-GoM inverse model, with setup files and instructions for running it can be accessed at: https://github.com/mstukel/N15-LIM-BLOOFINZ-GoM

REFERENCES

Alemany, F., Quintanilla, L., Velez-Belchí, P., García, A., Cortés, D., Rodríguez, J. M., de Puelles, M. F., González-Pola, C., et al. (2010) Characterization of the spawning habitat of Atlantic bluefin tuna and related species in the Balearic Sea (western Mediterranean). *Prog. Oceanogr.*, **86**, 21-38.

Alldredge, A. (1976) Field behavior and adaptive strategies of appendicularians (Chordata: Tunicata). *Mar. Biol.*, **38**, 29-39.

Arreguin-Sanchez, F., Zetina-Rejón, M., Manickchand-Heileman, S., Ramırez-Rodrıguez, M. and Vidal, L. (2004) Simulated response to harvesting strategies in an exploited ecosystem in the southwestern Gulf of Mexico. *Ecol. Model.*, **172**, 421-432.

Bakun, A. (2006) Fronts and eddies as key structures in the habitat of marine fish larvae: opportunity, adaptive response and competitive advantage. *Sci. Mar.*, **70**, 105-122.

Bakun, A. and Broad, K. (2003) Environmental 'loopholes' and fish population dynamics: comparative pattern recognition with focus on El Niño effects in the Pacific. *Fish. Oceanogr.*, **12**, 458-473.

Barton, A. D., Irwin, A. J., Finkel, Z. V. and Stock, C. A. (2016) Anthropogenic climate change drives shift and shuffle in North Atlantic phytoplankton communities. *Proc. Natl. Acad. Sci. U. S. A.*, **113**, 2964-2969.

Biggs, D. C. (1992) Nutrients, plankton, and productivity in a warm-core ring in the western Gulf of Mexico. *J. Geophys. Res. Oceans*, **97**, 2143-2154.

Biggs, D. C. and Müller-Karger, F. E. (1994) Ship and satellite observations of chlorophyll stocks in interacting cyclone-anticyclone eddy pairs in the western Gulf of Mexico. *J. Geophys. Res. Oceans*, **99**, 7371-7384.

Biggs, D. C. and Ressler, P. H. (2001) Distribution and abundance of phytoplankton, zooplankton, ichthyoplankton, and micronekton in the deepwater Gulf of Mexico. *Gulf Mex. Sci.*, **19**, 2.

Bode, M., Hagen, W., Schukat, A., Teuber, L., Fonseca-Batista, D., Dehairs, F. and Auel, H. (2015) Feeding strategies of tropical and

ACKNOWLEDGMENTS

- subtropical calanoid copepods throughout the eastern Atlantic Ocean Latitudinal and bathymetric aspects. *Prog. Oceanogr.*, **138**, 268-282.
- Boenigk, J. and Arndt, H. (2002) Bacterivory by heterotrophic flagellates: community structure and feeding strategies. *Anton. Leeuw. Int. J. G.*, **81**, 465-480.
- Bronk, D. A., Killberg-Thoreson, L., Sipler, R. E., Mulholland, M. R., Roberts, Q. N., Bernhardt, P. W., Garrett, M., O'Neil, J. M., et al. (2014) Nitrogen uptake and regeneration (ammonium regeneration, nitrification and photoproduction) in waters of the West Florida Shelf prone to blooms of *Karenia brevis*. *Harmful Algae*, **38**, 50-62.
- Calbet, A. (2008) The trophic roles of microzooplankton in marine systems. *ICES J. Mar. Sci.*, **65**, 325-331.
- Caron, D. A., Countway, P. D., Jones, A. C., Kim, D. Y. and Schnetzer, A. (2012) Marine Protistan Diversity. *Annu. Rev. Mar. Sci.*, **4**, 467-493.
- Catalán, I. A., Tejedor, A., Alemany, F. and Reglero, P. (2011) Trophic ecology of Atlantic bluefin tuna *Thunnus thynnus* larvae. *J. Fish Biol.*, **78**, 1545-1560.
- Ciannelli, L., Bailey, K. and Olsen, E. M. (2015) Evolutionary and ecological constraints of fish spawning habitats. *ICES J. Mar. Sci.*, **72**, 285-296.
- Clark, D. R., Rees, A. P. and Joint, I. (2008) Ammonium regeneration and nitrification rates in the oligotrophic Atlantic Ocean: Implications for new production estimates. *Limnol. Oceanogr.*, **53**, 52-62.
- Clark, D. R., Widdicombe, C. E., Rees, A. P. and Woodward, E. M. S. (2016) The significance of nitrogen regeneration for new production within a filament of the Mauritanian upwelling system. *Biogeosciences*, **13**, 2873-2888.
- Cornic, M., Smith, B. L., Kitchens, L. L., Bremer, J. R. A. and Rooker, J. R. (2018) Abundance and habitat associations of tuna larvae in the surface water of the Gulf of Mexico. *Hydrobiol.*, **806**, 29-46.
- Damien, P., Pasqueron de Fommervault, O., Sheinbaum, J., Jouanno, J., Camacho-Ibar, V. F. and Duteil, O. (2018) Partitioning of the open waters of the Gulf of Mexico based on the seasonal and interannual variability of chlorophyll concentration. *J. Geophys. Res. Oceans*, **123**, 2592-2614.
- Décima, M., Landry, M. R., Stukel, M. R., Lopez-Lopez, L. and Krause, J. W. (2016) Mesozooplankton biomass and grazing in the Costa Rica Dome: amplifying variability through the plankton food web. *J. Plankton Res.*, **38**, 317-330.
- Domingues, R., Goni, G., Bringas, F., Muhling, B., Lindo-Atichati, D. and Walter, J. (2016) Variability of preferred environmental conditions for Atlantic bluefin tuna (*Thunnus thynnus*) larvae in the Gulf of Mexico during 1993–2011. *Fish. Oceanogr.*, **25**, 320-336.
- Eppley, R. W. and Peterson, B. J. (1979) Particulate organic matter flux and planktonic new production in the deep ocean. *Nature*, **282**, 677-680.
- Flombaum, P., Gallegos, J. L., Gordillo, R. A., Rincón, J., Zabala, L. L., Jiao, N., Karl, D. M., Li, W. K. W., et al. (2013) Present and future global distributions of the marine Cyanobacteria *Prochlorococcus* and *Synechococcus*. *Proc. Natl. Acad. Sci. U. S. A.*, **110**, 9824-9829.
- Flynn, K. J., Stoecker, D. K., Mitra, A., Raven, J. A., Glibert, P. M., Hansen, P. J., Graneli, E. and Burkholder, J. M. (2013) Misuse of the phytoplankton-zooplankton dichotomy: the need to assign organisms as mixotrophs within plankton functional types. *J. Plankton Res.*, **35**, 3-11.
- Forristall, G. Z., Schaudt, K. J. and Cooper, C. K. (1992) Evolution and kinematics of a Loop Current eddy in the Gulf of Mexico during 1985. *J. Geophys. Res. Oceans*, **97**, 2173-2184.
- Fuchs, H. L. and Franks, P. J. S. (2010) Plankton community properties determined by nutrients and size-selective feeding. *Mar. Ecol. Prog. Ser.*, **413**, 1-15.

- García, A., Laiz-Carrión, R., Uriarte, A., Quintanilla, J. M., Morote, E., Rodríguez, J. M. and Alemany, F. (2017) Differentiated stable isotopes signatures between pre-and post-flexion larvae of Atlantic bluefin tuna (*Thunnus thynnus*) and of its associated tuna species of the Balearic Sea (NW Mediterranean). *Deep-Sea Res. II*, 140, 18-24.
- Gargett, A. and Garner, T. (2008) Determining Thorpe scales from ship-lowered CTD density profiles. *J. Atmos. and Ocean. Tech.*, **25**, 1657-1670.
- Geers, T. M., Pikitch, E. K. and Frisk, M. G. (2016) An original model of the northern Gulf of Mexico using Ecopath with Ecosim and its implications for the effects of fishing on ecosystem structure and maturity. *Deep-Sea Res. II*, **129**, 319-331.
- Gerard, T., Lamkin, J., Kelly, T. B., Knapp, A. N., Laiz-Carrión, R., Malca, E., Selph, K. E., Shiroza, A., et al. (this issue) Bluefin Larvae in Oligotrophic Ocean Foodwebs, Investigations of Nutrients to Zooplankton: Overview of the BLOOFINZ-Gulf of Mexico program. *J. Plankton Res.*
- Gomez, F. A., Lee, S.-K., Liu, Y., Hernandez Jr, F. J., Muller-Karger, F. E. and Lamkin, J. T. (2018) Seasonal patterns in phytoplankton biomass across the northern and deep Gulf of Mexico: a numerical model study. *Biogeosciences*, **15**, 3561-3576.
- Gorsky, G. and Fenaux, R. (1998) The role of Appendicularia in marine food webs. In: Bone (ed) *The biology of pelagic tunicates*. pp. 161-169.
- Hannon, B. (1973) Structure of ecosystems. *J. Theor. Biol.*, **41**, 535-546.
- Hong, H., Shen, R., Zhang, F., Wen, Z., Chang, S., Lin, W., Kranz, S. A., Luo, Y.-W., et al. (2017) The complex effects of ocean acidification on the prominent N2-fixing cyanobacterium *Trichodesmium. Science*, **356**, 527-531.
- Ikeda, T. (1985) Metabolic rates of epipelagic marine zooplankton as a function of body mass and temperature. *Mar. Biol.*, **85**, 1-11.
- Katechakis, A. and Stibor, H. (2004) Feeding selectivities of the marine cladocerans *Penilia avirostris*, *Podon intermedius* and *Evadne nordmanni*. *Mar. Biol.*, **145**, 529-539.
- Kelly, T. B., Landry, M. R., Selph, K. E., Knapp, A. N., Swalethorp, R. and Stukel, M. R. (in review) Lateral advection supports nitrogen export in the oligotrophic ecosystem of the open-ocean Gulf of Mexico. *Nature Communications*.
- Kim, S., Onbé, T. and Yoon, Y. (1989) Feeding habits of marine cladocerans in the Inland Sea of Japan. *Mar. Biol.*, **100**, 313-318. Kiørboe, T. (2008) *A Mechanistic Approach to Plankton Ecology*. Vol., Princeton University Press, Princeton, NJ.
- Kitchens, L. L. and Rooker, J. R. (2014) Habitat associations of dolphinfish larvae in the Gulf of Mexico. *Fish. Oceanogr.*, **23**, 460-471.
- Knapp, A. N., Thomas, R., Stukel, M. R., Kelly, T. B., Landry, M. R., Selph, K. E., Malca, E., Gerard, T., et al. (this issue) Constraining the sources of nitrogen fueling export production in the Gulf of Mexico using nitrogen isotope budgets. *J. Plankton Res*.
- Kones, J. K., Soetaert, K., van Oevelen, D. and Owino, J. O. (2009) Are network indices robust indicators of food web functioning? A Monte Carlo approach. *Ecol. Model.*, **220**, 370-382.
- Laiz-Carrión, R., Gerard, T., Suca, J. J., Malca, E., Uriarte, A., Quintanilla, J. M., Privoznik, S., Llopiz, J. K., et al. (2019) Stable isotope analysis indicates resource partitioning and trophic niche overlap in larvae of four tuna species in the Gulf of Mexico. *Mar. Ecol. Prog. Ser.*, **619**, 53-68.
- Laiz-Carrion, R., Gerard, T., Uriarte, A., Malca, E., Quintanilla, J. M., Muhling, B. A., Alemany, F., Privoznik, S. L., et al. (2015) Trophic Ecology of Atlantic Bluefin Tuna (*Thunnus thynnus*) Larvae from the Gulf of Mexico and NW Mediterranean Spawning Grounds: A Comparative Stable Isotope Study. *Plos One*, **10**.

- Landry, M. R., Beckley, L. E. and Muhling, B. A. (2019) Climate sensitivities and uncertainties in food-web pathways supporting larval bluefin tuna in subtropical oligotrophic oceans. *ICES J. Mar. Sci.*, **76**, 359-369
- Landry, M. R., Ohman, M. D., Goericke, R., Stukel, M. R. and Tsyrklevich, K. (2009) Lagrangian studies of phytoplankton growth and grazing relationships in a coastal upwelling ecosystem off Southern California. *Prog. Oceanogr.*, **83**, 208-216.
- Landry, M. R., Selph, K. E., Decima, M., Gutierrez-Rodriquez, A., Stukel, M. R., Taylor, A. G. and Pasulka, A. L. (2016) Phytoplankton production and grazing balances in the Costa Rica Dome. *J. Plankton Res.*, **38**, 366-379.
- Landry, M. R., Selph, K. E., Stukel, M. R., Swalethorp, R., Kelly, T. B., Beatty, J. and Quackenbush, C. R. (this issue) Microbial food web dynamics in the oceanic Gulf of Mexico. *J. Plankton Res.*
- Landry, M. R. and Swalethorp, R. (this issue) Mesozooplankton biomass, grazing and trophic structure in the bluefin tuna spawning area of the oceanic Gulf of Mexico. *J. Plankton Res.*
- Lindo-Atichati, D., Bringas, F., Goni, G., Muhling, B., Muller-Karger, F. E. and Habtes, S. (2012) Varying mesoscale structures influence larval fish distribution in the northern Gulf of Mexico. *Mar. Ecol. Prog. Ser.*, **463**, 245-257.
- Lipschultz, F. (2001) A time-series assessment of the nitrogen cycle at BATS. *Deep-Sea Res. II*, **48**, 1897-1924.
- Liu, Y., Lee, S.-K., Enfield, D. B., Muhling, B. A., Lamkin, J. T., Muller-Karger, F. E. and Roffer, M. A. (2015) Potential impact of climate change on the Intra-Americas Sea: Part-1. A dynamic downscaling of the CMIP5 model projections. *J. Mar. Sys.*, **148**, 56-69.
- Llopiz, J. K., Muhling, B. A. and Lamkin, J. T. (2015) Feeding dynamics of Atlantic Bluefin Tuna (*Thunnus thynnus*) larvae in the Gulf of Mexico. *Collect. Vol. Sci. Pap. ICCAT*, **71**, 1710-1715.
- Llopiz, J. K., Richardson, D. E., Shiroza, A., Smith, S. L. and Cowen, R. K. (2010) Distinctions in the diets and distributions of larval tunas and the important role of appendicularians. *Limnol. Oceanogr.*, **55**, 983-996.
- Malca, E., Muhling, B., Franks, J., García, A., Tilley, J., Gerard, T., Ingram Jr, W. and Lamkin, J. T. (2017) The first larval age and growth curve for bluefin tuna (*Thunnus thynnus*) from the Gulf of Mexico: comparisons to the Straits of Florida, and the Balearic Sea (Mediterranean). *Fisheries Research*, **190**, 24-33.
- Malca, E., Swalethorp, R., Quintanilla, J. M., Laiz-Carrión, R., Shropshire, T. A., Kelly, T. B., Shiroza, A., Stukel, M. R., et al. (in prep.) Influence of habitat and food quality on growth rate of bluefin tuna larvae in the Gulf of Mexico. *J. Plankton Res.*, **this issue**.
- Mauchline, J. (1998) *Adv. Mar. Biol.: The biology of calanoid copepods.* Vol. 33, Academic Press, San Diego.
- McCarthy, J. J., Garside, C., Nevins, J. L. and Barber, R. T. (1996) New production along 140°W in the equatorial Pacific during and following the 1992 El Niño event. *Deep-Sea Res. II*, **43**, 1065-1093.
- Muhling, B. A., Lamkin, J. T., Alemany, F., García, A., Farley, J., Ingram, G. W., Berastegui, D. A., Reglero, P., et al. (2017) Reproduction and larval biology in tunas, and the importance of restricted area spawning grounds. *Rev. Fish. Biol. Fisheries*, **27**, 697-732.
- Muhling, B. A., LAMKIN, J. T. and ROFFER, M. A. (2010) Predicting the occurrence of Atlantic bluefin tuna (*Thunnus thynnus*) larvae in the northern Gulf of Mexico: building a classification model from archival data. *Fish. Oceanogr.*, **19**, 526-539.
- Muhling, B. A., Lee, S.-K., Lamkin, J. T. and Liu, Y. (2011) Predicting the effects of climate change on bluefin tuna (*Thunnus thynnus*) spawning habitat in the Gulf of Mexico. *ICES J. Mar. Sci.*, **68**, 1051-1062.

- Muhling, B. A., Liu, Y., Lee, S.-K., Lamkin, J. T., Roffer, M. A., Muller-Karger, F. and Walter III, J. F. (2015) Potential impact of climate change on the Intra-Americas Sea: Part 2. Implications for Atlantic bluefin tuna and skipjack tuna adult and larval habitats. *J. Mar. Sys.*. **148**, 1-13.
- Muller-Karger, F. E., Smith, J. P., Werner, S., Chen, R., Roffer, M., Liu, Y., Muhling, B., Lindo-Atichati, D., et al. (2015) Natural variability of surface oceanographic conditions in the offshore Gulf of Mexico. *Prog. Oceanogr.*, **134**, 54-76.
- Newell, S. E., Fawcett, S. E. and Ward, B. B. (2013) Depth distribution of ammonia oxidation rates and ammonia-oxidizer community composition in the Sargasso Sea. *Limnol. Oceanogr.*, **58**, 1491-1500.
- Oey, L., Ezer, T. and Lee, H. (2005) Loop Current, rings and related circulation in the Gulf of Mexico: A review of numerical models and future challenges. *Geophys. Monogr.-AGU*, **161**, 31-56.
- Pomeroy, L. R., Williams, P. J. I., Azam, F. and Hobbie, J. E. (2007) The Microbial Loop. *Oceanography*, **20**, 28-33.
- Reglero, P., Santos, M., Balbín, R., Laíz-Carrión, R., Alvarez-Berastegui, D., Ciannelli, L., Jiménez, E. and Alemany, F. (2017) Environmental and biological characteristics of Atlantic bluefin tuna and albacore spawning habitats based on their egg distributions. *Deep-Sea Res. II*, **140**, 105-116.
- Rodríguez-Ezpeleta, N., Díaz-Arce, N., Walter III, J. F., Richardson, D. E., Rooker, J. R., Nøttestad, L., Hanke, A. R., Franks, J. S., et al. (2019) Determining natal origin for improved management of Atlantic bluefin tuna. *Front. Ecol. Environ.*, **17**, 439-444.
- Rooker, J. R., Bremer, J. R. A., Block, B. A., Dewar, H., De Metrio, G., Corriero, A., Kraus, R. T., Prince, E. D., et al. (2007) Life history and stock structure of Atlantic bluefin tuna (*Thunnus thynnus*). *Reviews in Fisheries Science*, **15**, 265-310.
- Rooker, J. R., Kitchens, L. L., Dance, M. A., Wells, R. D., Falterman, B. and Cornic, M. (2013) Spatial, temporal, and habitat-related variation in abundance of pelagic fishes in the Gulf of Mexico: potential implications of the Deepwater Horizon oil spill. *PloS one*, **8**, e76080.
- Rooker, J. R., Simms, J. R., Wells, R. D., Holt, S. A., Holt, G. J., Graves, J. E. and Furey, N. B. (2012) Distribution and habitat associations of billfish and swordfish larvae across mesoscale features in the Gulf of Mexico. *PloS one*, **7**, e34180.
- Rost, B., Zondervan, I. and Wolf-Gladrow, D. (2008) Sensitivity of phytoplankton to future changes in ocean carbonate chemistry: current knowledge, contradictions and research directions. *Mar. Ecol. Prog. Ser.*, **373**, 227-237.
- Saint-Béat, B., Vézina, A. F., Asmus, R., Asmus, H. and Niquil, N. (2013) The mean function provides robustness to linear inverse modelling flow estimation in food webs: A comparison of functions derived from statistics and ecological theories. *Ecol. Model.*, **258**, 53-64.
- Scanlan, D. J. and Post, A. F. (2008) Chapter 24 Aspects of Marine Cyanobacterial Nitrogen Physiology and Connection to the Nitrogen Cycle. In: D. G. Capone, D. A. Bronk, M. R. Mulholland and E. J. Carpenter (eds) *Nitrogen in the Marine Environment (2nd Edition)*. Academic Press, San Diego, pp. 1073-1095.
- Schmitz, W., Biggs, D., Lugo-Fernandez, A., Oey, L. Y. and Sturges, W. (2005) A synopsis of the circulation in the Gulf of Mexico and on its continental margins. *Circulation in the Gulf of Mexico: Observations and models*, 11-29.
- Selph, K. E., Landry, M. R., Taylor, A. G., Gutierrez-Rodriguez, A., Stukel, M. R., Wokuluk, J. and Pasulka, A. (2016) Phytoplankton production and taxon-specific growth rates in the Costa Rica Dome. *J. Plankton Res.*, **38**, 199-215.
- Selph, K. E., Swalethorp, R., Stukel, M. R., Kelly, T. B., Knapp, A. N., Fleming, K., Hernandez, T. and Landry, M. R. (this issue)

- Phytoplankton community composition and biomass in the oligotrophic Gulf of Mexico. *J. Plankton Res.*
- Sherr, E. B. and Sherr, B. F. (2016) Phagotrophic protists: central roles in microbial food webs. In: P. M. Glibert and T. M. Kana (eds) *Aquatic Microbial Ecology and Biogeochemistry: A Dual Perspective*. Springer, pp. 3-12.
- Shiozaki, T., Ijichi, M., Isobe, K., Hashihama, F., Nakamura, K.-i., Ehama, M., Hayashizaki, K.-i., Takahashi, K., et al. (2016) Nitrification and its influence on biogeochemical cycles from the equatorial Pacific to the Arctic Ocean. *ISME J.*, **10**, 2184-2197.
- Shiroza, A., Malca, E., Lamkin, J., Gerard, T., Landry, M. R., Stukel, M. R., Laiz-Carrión, R. and Swalethorp, R. (this issue) Active prey selection in developing larvae of Atlantic bluefin tuna (*Thunnus thynnus*) in spawning grounds of the Gulf of Mexico. *J. Plankton Res.*
- Shropshire, T. A., Morey, S. L., Chassignet, E., Coles, V. J., Fiksen, O., Gerard, T., Malca, E., Laiz-Carrión, R., et al. (this issue) Trade-offs between risks of predation and starvation in larvae make the shelf break an optimal spawning location for Atlantic Bluefin tuna. *J. Plankton Res.*
- Shropshire, T. A., Morey, S. L., Chassignet, E. P., Bozec, A., Coles, V. J., Landry, M. R., Swalethorp, R., Zapfe, G., et al. (2020) Quantifying spatiotemporal variability in zooplankton dynamics in the Gulf of Mexico with a physical-biogeochemical model. *Biogeosciences*, 17, 3385-3407.
- Smith, J. M., Chavez, F. P. and Francis, C. A. (2014) Ammonium uptake by phytoplankton regulates nitrification in the sunlit ocean. *Plos One*, **9**, e108173.
- Soetaert, K., Van den Meersche, K. and van Oevelen, D. (2009) limSolve: Solving linear inverse models *R package version 1.5.4*.
- Stoecker, D. K., Hansen, P. J., Caron, D. A. and Mitra, A. (2017) Mixotrophy in the Marine Plankton. *Annu. Rev. Mar. Sci.*, **9**, 311-335.
- Strickland, J. D. and Parsons, T. R. (1972) A practical handbook of seawater analysis, second ed. *Bull. Fish. Res. Board Can.*, **167**.
- Stukel, M. R., Décima, M. and Kelly, T. B. (2018a) A new approach for incorporating 15N isotopic data into linear inverse ecosystem models with Markov Chain Monte Carlo sampling. *PloS one*, **13**, e0199123.
- Stukel, M. R., Décima, M., Landry, M. R. and Selph, K. E. (2018b) Nitrogen and isotope flows through the Costa Rica Dome upwelling ecosystem: The crucial mesozooplankton role in export flux. *Global Biogeochem. Cycles*, **32**, 1815-1832.
- Stukel, M. R., Kahru, M., Benitez-Nelson, C. R., Decima, M., Goericke, R., Landry, M. R. and Ohman, M. D. (2015) Using Lagrangian-based process studies to test satellite algorithms of vertical carbon flux in the eastern North Pacific Ocean. *J. Geophys. Res. Oceans*, **120**, 7208-7222.
- Stukel, M. R., Kelly, T. B., Landry, M. R., Selph, K. E. and Swalethorp, R. (this issue) Sinking carbon, nitrogen, and pigment flux within and beneath the euphotic zone in the oligotrophic, open-ocean Gulf of Mexico. *J. Plankton Res*.
- Stukel, M. R., Landry, M. R., Ohman, M. D., Goericke, R., Samo, T. and Benitez-Nelson, C. R. (2012) Do inverse ecosystem models accurately reconstruct plankton trophic flows? Comparing two solution methods using field data from the California Current. *J. Mar. Sys.*, **91**, 20-33.
- Taylor, A. G. and Landry, M. R. (2018) Phytoplankton biomass and size structure across trophic gradients in the southern California Current and adjacent ocean ecosystems. *Mar. Ecol. Prog. Ser.*, **592**, 1-17
- Teo, S. L., Boustany, A., Dewar, H., Stokesbury, M. J., Weng, K. C., Beemer, S., Seitz, A. C., Farwell, C. J., et al. (2007) Annual

- migrations, diving behavior, and thermal biology of Atlantic bluefin tuna, *Thunnus thynnus*, on their Gulf of Mexico breeding grounds. *Mar. Biol.*, **151**, 1-18.
- Tilley, J. D., Butler, C. M., Suárez-Morales, E., Franks, J. S., Hoffmayer, E. R., Gibson, D. P., Comyns, B. H., Ingram Jr, G. W., et al. (2016) Feeding ecology of larval Atlantic bluefin tuna, *Thunnus thynnus*, from the central Gulf of Mexico. *Bull. Mar. Sci.*, **92**, 321-334.
- Turner, J. T. (1986) Zooplankton feeding ecology: contents of fecal pellets of the cyclopoid copepods *Oncaea venusta*, *Corycaeus amazonicus*, *Oithona plumifera*, and *O. simplex* from the northern Gulf of Mexico. *Mar. Ecol.*, **7**, 289-302.
- Uriarte, A., Johnstone, C., Laiz-Carrión, R., García, A., Llopiz, J. K., Shiroza, A., Quintanilla, J. M., Lozano-Peral, D., et al. (2019) Evidence of density-dependent cannibalism in the diet of wild Atlantic bluefin tuna larvae (*Thunnus thynnus*) of the Balearic Sea (NW-Mediterranean). *Fisheries Research*, **212**, 63-71.
- Uye, S.-i. and Kayano, Y. (1994) Predatory feeding behavior of Tortanus (Copepoda: Calanoida): life-stage differences and the predation impact on small planktonic crustaceans. *J. Crust. Biol.*, **14**, 473-483.
- Van den Meersche, K., Soetaert, K. and Van Oevelen, D. (2009) xSample(): An R function for sampling linear inverse problems. *J. Stat. Softw., Code Snippets*, **30**, 1-15.
- van Oevelen, D., Van den Meersche, K., Meysman, F. J. R., Soetaert, K., Middelburg, J. J. and Vezina, A. F. (2010) Quantifying food web flows using linear inverse models. *Ecosystems*, **13**, 32-45.
- Vézina, A. F. and Platt, T. (1988) Food web dynamics in the ocean .1. Best estimates of flow networks using inverse methods. *Mar. Ecol. Prog. Ser.*, **42**, 269-287.
- Walters, C., Martell, S. J., Christensen, V. and Mahmoudi, B. (2008) An Ecosim model for exploring Gulf of Mexico ecosystem management options: implications of including multistanza life-history models for policy predictions. *Bull. Mar. Sci.*, **83**, 251-271.
- Wan, X. S., Sheng, H.-X., Dai, M., Zhang, Y., Shi, D., Trull, T. W., Zhu, Y., Lomas, M. W., et al. (2018) Ambient nitrate switches the ammonium consumption pathway in the euphotic ocean. *Nature communications*, **9**, 1-9.
- Wells, R. D., Rooker, J. R., Quigg, A. and Wissel, B. (2017) Influence of mesoscale oceanographic features on pelagic food webs in the Gulf of Mexico. *Mar. Biol.*, **164**, 92.
- Xu, M. N., Li, X., Shi, D., Zhang, Y., Dai, M., Huang, T., Glibert, P. M. and Kao, S. J. (2019) Coupled effect of substrate and light on assimilation and oxidation of regenerated nitrogen in the euphotic ocean. *Limnol. Oceanogr.*, **64**, 1270-1283.
- Yingling, N., Kelly, T. B., Selph, K. E., Landry, M. R., Knapp, A. N., Kranz, S. A. and Stukel, M. R. (this issue) Taxon-specific phytoplankton growth, nutrient limitation, and light limitation in the oligotrophic Gulf of Mexico. *J. Plankton Res.*
- Yool, A., Martin, A. P., Fernandez, C. and Clark, D. R. (2007) The significance of nitrification for oceanic new production. *Nature*, **447**, 999-1002.
- Zehr, J. P. (2011) Nitrogen fixation by marine cyanobacteria. *Trends Microbiol.*, **19**, 162-173.

Table 1. Rate, biomass, and $\delta^{15}N$ measurements used as inputs to the inverse model.

Rate Measurements	Units	Cycle 1	Cycle 5	Source
NPP (shallow)	mmol N m ⁻² d ⁻¹	2.23 ± 0.13	3.08 ± 0.14	Yingling <i>et al.</i> (this issue)
NPP (deep)	mmol N m ⁻² d ⁻¹	1.64 ± 0.07	1.34 ± 0.05	Yingling <i>et al.</i> (this issue)
f-ratio (shallow)	mmol N m ⁻² d ⁻¹	0.06 ± 0.04	0.14 ± 0.04	Yingling <i>et al.</i> (this issue)
f-ratio (deep)	mmol N m ⁻² d ⁻¹	0.44 ± 0.3	0.09 ± 0.02	Yingling <i>et al.</i> (this issue)
Protistan Grazing Rate (shallow)	mmol N m ⁻² d ⁻¹	1.72 ± 0.6	2.58 ± 0.14	Yingling <i>et al.</i> (this issue)
Protistan Grazing Rate (deep)	mmol N m ⁻² d ⁻¹	1.44 ± 0.48	0.66 ± 0.18	Yingling <i>et al.</i> (this issue)
Picophyto NPP (shallow)	mmol N m ⁻² d ⁻¹	1.15 ± 0.21	2.38 ± 0.37	Landry et al. (this issue)
Picophyto NPP (deep)	mmol N m ⁻² d ⁻¹	0.78 ± 0.15	1.02 ± 0.17	Landry et al. (this issue)
Flagellate NPP (shallow)	mmol N m ⁻² d ⁻¹	1.01 ± 0.37	0.69 ± 0.17	Landry et al. (this issue)
Flagellate NPP (deep)	mmol N m ⁻² d ⁻¹	0.83 ± 0.35	0.32 ± 0.13	Landry et al. (this issue)
Diatom NPP (shallow)	mmol N m ⁻² d ⁻¹	0.08 ± 0.03	0.01 ± 0	Landry et al. (this issue)
Diatom NPP (deep)	mmol N m ⁻² d ⁻¹	0.02 ± 0.02	0 ± 0	Landry et al. (this issue)
Picophyto Mortality (shallow)	mmol N m ⁻² d ⁻¹	0.71 ± 0.32	1.6 ± 0.12	Landry et al. (this issue)
Picophyto Mortality (deep)	mmol N m ⁻² d ⁻¹	0.43 ± 0.07	0.34 ± 0.09	Landry et al. (this issue)
Flagellate Mortality (shallow)	mmol N m ⁻² d ⁻¹	0.86 ± 0.26	0.19 ± 0.11	Landry et al. (this issue)
Flagellate Mortality (deep)	mmol N m ⁻² d ⁻¹	0.6 ± 0.17	0.04 ± 0.02	Landry et al. (this issue)
Diatom Mortality (shallow)	mmol N m ⁻² d ⁻¹	0.04 ± 0.02	0.01 ± 0	Landry et al. (this issue)
Diatom Mortality (deep)	mmol N m ⁻² d ⁻¹	0.01 ± 0.01	0 ± 0	Landry et al. (this issue)
NVM Mesozoo Grazing	mmol N m ⁻² d ⁻¹	0.39 ± 0.1	0.52 ± 0.1	Landry & Swalethorp (this issue)
VM Mesozoo Grazing	mmol N m ⁻² d ⁻¹	0.03 ± 0.06	0.15 ± 0.08	Landry & Swalethorp (this issue)
SedTrap Flux (shallow)	mmol N m ⁻² d ⁻¹	1.53 ± 0.55	1.08 ± 0.07	Stukel et al. (this issue)
SedTrap Flux (deep)	mmol N m ⁻² d ⁻¹	0.46 ± 0.02	0.87 ± 0.18	Stukel et al. (this issue)
Chl Sinking (shallow)	mmol N m ⁻² d ⁻¹	0.02 ± 0.02	0.03 ± 0.02	Stukel et al. (this issue)
Chl Sinking (deep)	mmol N m ⁻² d ⁻¹	0.02 ± 0.01	0.05 ± 0.04	Stukel et al. (this issue)
Fecal Pellet Sinking (shallow)	mmol N m ⁻² d ⁻¹	0.03 ± 0.03	0.02 ± 0.02	Stukel et al. (this issue)
Fecal Pellet Sinking (deep)	mmol N m ⁻² d ⁻¹	0.13 ± 0.06	0.25 ± 0.2	Stukel et al. (this issue)
Microzoo to Preflex	nmol N m ⁻² d ⁻¹	0.34 ± 0.16	0 ± 0.01	Shiroza et al. (this issue)
Microzoo to Postflex	nmol N m ⁻² d ⁻¹	5.45 ± 0.88	0 ± 0.01	Shiroza et al. (this issue)
Appendicularian to Preflex	nmol N m ⁻² d ⁻¹	0.77 ± 0.32	0.04 ± 0.03	Shiroza et al. (this issue)
Appendicularian to Postflex	nmol N m ⁻² d ⁻¹	6.75 ± 0.47	1.88 ± 0.2	Shiroza et al. (this issue)
Cladoceran to Preflex	nmol N m ⁻² d ⁻¹	0.16 ± 0.16	0.78 ± 0.25	Shiroza et al. (this issue)
Cladoceran to Postflex	nmol N m ⁻² d ⁻¹	23.43 ± 2.26	26.47 ± 2.78	Shiroza et al. (this issue)
Calanoids to Preflex	nmol N m ⁻² d ⁻¹	3.61 ± 1.34	1.87 ± 0.35	Shiroza <i>et al.</i> (this issue)
Calanoids to Postflex	nmol N m ⁻² d ⁻¹	63.62 ± 0.96	13.49 ± 0.32	Shiroza <i>et al.</i> (this issue)
Poecilastomatoids to Preflex	nmol N m ⁻² d ⁻¹	0 ± 0.01	0 ± 0.01	Shiroza <i>et al.</i> (this issue)
Poecilastomatoids to Postflex	nmol N m ⁻² d ⁻¹	1.74 ± 2.63	0.89 ± 0.03	Shiroza et al. (this issue)
Biomass and other measurements				
Temperature (0-50)	°C	24.31	24.44	CTD
Temperature (50-120)	°C	22.14	21.68	CTD
Temperature (120-300)	°C	16.41	16.46	CTD
HerbNVM biomass (shallow)	μmol N m ⁻²	23.24	45.63	Shiroza et al. (this issue)
App Biomass (shallow)	μmol N m ⁻²	0.22	0.32	Shiroza <i>et al.</i> (this issue)
Clad Biomass (shallow)	μmol N m ⁻²	0.06	0.12	Shiroza et al. (this issue)
NVM Cal Biomass (shallow)	μmol N m ⁻²	103.09	126.89	Shiroza et al. (this issue)
Chaeto Biomass (shallow)	μmol N m ⁻²	107.04	130.13	Shiroza et al. (this issue)
Poecil Biomass (shallow)	μmol N m ⁻²	28.65	18.53	Shiroza et al. (this issue)
Preflex Biomass (shallow)	μmol N m ⁻²	0.06	1.18	Shiroza et al. (this issue)
Postflex Biomass (shallow)	μmol N m ⁻²	0.62	1.91	Shiroza et al. (this issue)
HerbVM Biomass	μmol N m ⁻²	88.62	-	Shiroza et al. (this issue)
vmCal Biomass	μmol N m ⁻²	78.29	-	Shiroza et al. (this issue)
Cyano Biomass (shallow)	mmol N m ⁻²	9.39	18.39	Selph et al. (this issue)
Tricho Biomass (shallow)	μmol N m ⁻²	27.23	0.97	Selph et al. (this issue)
Diatom Biomass (shallow)	mmol N m ⁻²	0.13	0.08	Selph et al. (this issue)
Flag Biomass (shallow)	mmol N m ⁻²	4.84	2.74	Selph et al. (this issue)
Cyano Biomass (deep)	mmol N m ⁻²	8.22	6.77	Selph et al. (this issue)
Tricho Biomass (deep)	μmol N m ⁻²	0.77	0.11	Selph et al. (this issue)

Diatom Biomass (deep)	mmol N m ⁻²	0.12	0.04	Selph et al. (this issue)
Flag Biomass (deep)	mmol N m ⁻²	6.97	3.63	Selph et al. (this issue)
HerbNVM Size	μg C ind ⁻¹	1.35	1.35	Shiroza et al. (this issue)
App Size	μg C ind-1	0.07	0.07	Shiroza et al. (this issue)
Clad Size	μg C ind-1	0.68	0.68	Shiroza et al. (this issue)
NVM Cal Size	μg C ind-1	4.44	4.44	Shiroza et al. (this issue)
Chaeto Size	μg C ind ⁻¹	20.83	20.83	Shiroza et al. (this issue)
Poecil Size	μg C ind ⁻¹	5.33	5.33	Shiroza et al. (this issue)
Preflex Size	μg C ind-1	83.71	83.71	Shiroza et al. (this issue)
Postflex Size	μg C ind-1	179.75	179.75	Shiroza et al. (this issue)
HerbVM Size	μg C ind-1	4.44	4.44	Shiroza et al. (this issue)
vmCal Size	μg C ind ⁻¹	4.44	4.44	Shiroza et al. (this issue)
Maximum upwelling rate (shallow)	μ mol N m ⁻² d ⁻¹	0.09	0.09	Kelly et al. (in review)
Maximum upwelling rate (deep)	μmol N m ⁻² d ⁻¹	366.79	1543.33	Kelly et al. (in review)
Maximum lateral advection of PON	mmol N m ⁻² d ⁻¹	3.22	3.22	Kelly et al. (in review)
Maximum lateral advection of DON	mmol N $m^{-2} d^{-1}$	1.56	1.56	Kelly et al. (in review)
δ^{15} N Values	0155 × (04.)			
Upwelled Nitrate	$\delta^{15}N_{AIR}$ (%)	3.20	2.90	Knapp et al. (this issue)
Preflex ABT	$\delta^{15}N_{AIR}$ (‰)	4.63	7.50	Swalethorp et al. (unpub.)
Postflex ABT	$\delta^{15}N_{AIR}$ (‰)	4.21	6.16	Swalethorp et al. (unpub.)
Shallow SedTrap	$\delta^{15} N_{AIR}$ (‰)	2.90	3.80	Stukel et al. (this issue)
Deep SedTrap	$\delta^{15}N_{AIR}$ (‰)	4.89	4.55	Stukel et al. (this issue)
Shallow DON	$\delta^{15}N_{AIR}$ (‰)	3.37	3.27	Knapp et al. (this issue)
Deep DON	$\delta^{15}N_{AIR}$ (‰)	3.31	3.39	Knapp et al. (this issue)
Shallow PON	$\delta^{15} N_{AIR}$ (‰)	1.44	2.66	Stukel et al. (this issue)
Deep PON	$\delta^{15}N_{AIR}$ (‰)	1.80	1.63	Stukel et al. (this issue)
Appendicularian	$\delta^{15} N_{AIR}$ (‰)	2.42	5.12	Swalethorp et al. (unpub).
Calanoid copepods	$\delta^{15}N_{AIR}$ (‰)	3.12	4.67	Swalethorp et al. (unpub).
Chaetognaths	$\delta^{15}N_{AIR}$ (‰)	5.70	7.58	Swalethorp et al. (unpub).
HerbVM	$\delta^{15} N_{AIR}$ (‰)	4.73	5.88	Swalethorp et al. (unpub).
HerbNVM	$\delta^{15} N_{AIR}$ (‰)	3.22	3.98	Swalethorp et al. (unpub).
Poecilostomatoids	$\delta^{15} N_{AIR}$ (‰)	-	6.29	Swalethorp et al. (unpub).
Cladocerans	$\delta^{15}N_{AIR}$ (‰)	1.48	5.16	Swalethorp et al. (unpub).

Supplementary Text – Online Appendix 1

Inverse model implementation

To constrain the flux of nitrogen through unmeasured ecosystem pathways, we used linear inverse ecosystem modeling (LIEM) techniques (Vézina and Platt, 1988; van Oevelen et al., 2010). LIEM allows investigators to specify mass balance constraints that must be exactly fit by food web solutions $(A\vec{x} = \vec{b})$, approximate equations that quantify measured rates with associated measurement uncertainty ($E\vec{x} \approx$ \vec{f}), and inequality constraints ($\vec{G}\vec{x} \ge \vec{h}$) that represent a priori acceptable ranges for different ecosystem properties. In these equations, \vec{x} represents the vector of food web flows that must be solved. For instance, in our model the first food web flux represents upwelling of nitrate from the deep euphotic zone to the shallow euphotic zone. Other food web fluxes include such things as nitrogen fixation by Trichodesmium in the upper euphotic zone, grazing of appendicularians on heterotrophic bacteria in the lower euphotic zone, ammonium excretion by preflexion ABT, and sinking flux of large detritus leaving the lower euphotic zone. Our model includes a total of 302 food web flows to be solved for (i.e., \vec{x} encodes 302 food web fluxes, see Fig. 1 and Supp. Table 1).

In the equation $A\vec{x} = \vec{b}$, the matrix A encodes mass balance constraints for all 44 model compartments (e.g., nitrate in the upper euphotic zone; poecilostomatoid copepods in the lower euphotic zone) and \vec{b} is a vector of zeroes, because we assume that the ecosystem is at steady state. These mass balance constraints will be exactly fit by all solution vectors, as explained below.

The approximate equation $E\vec{x} \approx \vec{f}$ encodes two types of information. The first is direct in situ field measurements that are connected to distinct model flows. For instance, protistan grazing on cyanobacteria measured in the upper euphotic zone by the dilution approach (Landry *et al.*, this issue) is equal to the sum of heterotrophic nanoflagellates grazing on cyanobacteria + microzooplankton grazing on cyanobacteria + mixotrophic flagellates grazing on cyanobacteria in this layer. The model included 38 such direct measurement constraints. Because these rates are measured with uncertainty, the model is not forced to match them exactly.

The other type of data encoded within $E\vec{x} \approx \vec{f}$ are mass balance constraints for flows of ¹⁵N for each compartment (44 additional approximate equalities). Because fluxes of ¹⁵N through the ecosystem are impacted by isotopic fractionation with uncertain fractionation coefficients, we incorporate these mass balance constraints using approximate equality constraints, rather than exact equality constraints (Stukel *et al.*, 2018a; Stukel *et al.*, 2018b).

The inequality $G\vec{x} \ge \vec{h}$ encodes known constraints on organisms and/or the ecosystem as a whole (e.g., gross growth efficiency of zooplankton is between 10% and 40%, all food web fluxes must be positive, respiration must be greater than a temperature-dependent function of biomass). All model solutions must fit within these greater than/less than constraints. We included 533 such inequality constraints. Note that all of the exact equalities, inequalities, and approximate equalities can be found (along with the code needed to run the model) in

a GitHub repository (https://github.com/mstukel/N15-LIM-BLOOFINZ-GoM). The inequalities, equalities, and approximate qualities specifically are found in the excel file 'N15InverseModelRW.GoM.xlsx' in the repository.

Despite the large number of constraints included in this modeling study, with 302 total unknown food web flows (\vec{x}), the system remains under-constrained. To objectively determine a representative solution (and confidence limits), we used the Markov Chain Monte Carlo (MCMC) with ¹⁵N approach (Stukel et al., 2018a; Stukel et al., 2018b). The MCMC approach initially uses the exact mass balance constraints $(A\vec{x} = \vec{b})$ to remove degrees of freedom from the solution and then creates bounds on the solution as formed by the hyperplanes prescribed by the inequality constraints ($G\vec{x} \ge \vec{h}$) (Kones et al., 2009; Soetaert et al., 2009; Van den Meersche et al., 2009). Then, starting with an initial guess of the solution that satisfies the equality and inequality constraints, the MCMC approach conducts a random walk through the solution space bounded by $A\vec{x} = \vec{b}$ and $G\vec{x} \ge \vec{h}$. New solutions are accepted based on the relative misfits of the new and previous solution with respect to the approximate equality measurements ($\vec{E}\vec{x} \approx \vec{f}$) and the uncertainty associated with the measurements codified in this approximate equation (Van den Meersche et al., 2009; Stukel et al., 2018a). This generates a set of solutions satisfying the equality and inequality constraints. The probability of inclusion for a specific solution is related to how well it satisfies the combined field measurement and 15N mass balance constraints. The arithmetic mean solution of the MCMC approach has been shown to more accurately recover withheld measurement constraints than the previously used L₂ minimum norm approach (Stukel et al., 2012; Saint-Béat et al., 2013). The MCMC+15N approach used herein builds on this previous work, but allows for the incorporation of non-linear constraints associated with unknown $\delta^{15}N$ values for some organisms or non-living nitrogen pools in the ecosystem to further constrain the system. This approach uses a second varying solution vector $(\vec{\delta})$ quantifying the ¹⁵N isotope fraction for each unknown nitrogen pool. A new solution set for $\vec{\delta}$ is determined at the same time as the new solution set for \vec{x} . $\vec{\delta}$ modifies the 44 approximate equality constraints that are associated with ¹⁵N mass balance. For additional details, see Stukel et al. (2018a).

For the model implementation used in this study, we included "weights" for different model flows that were related to the expected magnitude of each flow (i.e., we multiplied \vec{x} by a vector of weights and divided the rows of \boldsymbol{A} , \boldsymbol{G} , and \boldsymbol{E} by the same vector of weights). This was done to approximately normalize the magnitude of all flows in \vec{x} to maximize computational efficiency and was necessary because some flows (e.g., ammonium uptake by cyanobacteria) were many orders of magnitude larger than other flows (e.g., preflexion ABT feeding on poecilostomatoid copepods). For each cycle, we computed approximately 100 million solution vectors during the MCMC+15N procedure. We then thinned the solution set by only retaining every 10,000th solution vector to avoid autocorrelation, and removed the first 20% of the solution vectors (i.e., the first 20 million solution vectors) as a burn-in period. Jump lengths (e.g., the distance traveled from one solution vector to the next proposed solution vector) were tuned to ensure approximately 30% acceptance rates of new solutions.

Supplementary Table 1 – Model Solutions (mmol N m^{-2} d^{-1}) for each process, model layer (upper euphotic zone (UEZ), deep chlorophyll maximum (DCM), and Twilight zones), during Cycles 1 and 5.

Process	Model Layer	Cycle 1	Cycle 5
Upwelled NO₃	UEZ	4.37E-5 ± 2.51E-5	4.34E-5 ± 2.50E-5
Lateral Input of DON	UEZ	0.187 ± 0.123	0.1 ± 0.098
Lateral Input of PON	UEZ	0.179 ± 0.137	0.943 ± 0.329
Nitrification	UEZ	0.445 ± 0.177	0.792 ± 0.246
N ₂ fixation by PICO	UEZ	0.09 ± 0.085	0.06 ± 0.059
NO₃ uptake by PICO	UEZ	0.17 ± 0.139	0.363 ± 0.259
NH ₄ uptake by PICO	UEZ	1.528 ± 0.332	3.64 ± 0.391
PICO ==> HNF	UEZ	0.462 ± 0.27	0.958 ± 0.521
PICO ==> MIC	UEZ	0.273 ± 0.2	0.888 ± 0.517
PICO ==> FLAG	UEZ	2.18E-4 ± 1.74E-4	3.69E-4 ± 2.95E-4
PICO ==> APP	UEZ	2.65E-4 ± 1.70E-4	3.97E-4 ± 2.65E-4
DON exudation by TRICHO	UEZ	0.502 ± 0.185	1.336 ± 0.183
TRICHO mortality	UEZ UEZ	0.55 ± 0.262	0.881 ± 0.191
N2 fixation by TRICHO NO3 uptake by TRICHO	UEZ	1.90E-3 ± 9.24E-4 1.73E-3 ± 1.21E-3	5.57E-5 ± 3.88E-5 6.51E-5 ± 4.69E-5
NH4 uptake by TRICHO	UEZ	1.66E-3 ± 1.13E-3	6.39E-5 ± 4.62E-5
DON exudation by TRICHO	UEZ	2.71E-3 ± 1.62E-3	9.20E-5 ± 5.79E-5
TRICHO mortality	UEZ	2.57E-3 ± 1.53E-3	9.28E-5 ± 5.78E-5
NO3 uptake by DTM	UEZ	8.07E-2 ± 4.58E-2	8.67E-3 ± 4.99E-3
NH4 uptake by DTM	UEZ	7.16E-2 ± 4.85E-2	7.79E-3 ± 4.92E-3
DTM ==> MIC	UEZ	3.10E-2 ± 1.35E-2	1.82E-3 ± 1.49E-3
DTM ==> HERBnvm	UEZ	3.31E-3 ± 5.93E-4	1.06E-3 ± 9.48E-4
DTM ==> HERBvm	UEZ	1.33E-2 ± 1.14E-2	1.10E-3 ± 1.05E-3
DTM ==> APP	UEZ	1.97E-4 ± 1.56E-4	2.46E-4 ± 2.25E-4
DTM ==> CLAD	UEZ	1.25E-4 ± 7.91E-5	1.37E-4 ± 1.08E-4
DTM ==> nvmCAL	UEZ	6.57E-3 ± 3.73E-3	1.10E-3 ± 1.01E-3
DTM ==> vmCAL	UEZ	1.42E-2 ± 1.26E-2	1.12E-3 ± 1.06E-3
DON exudation by DTM	UEZ	3.53E-2 ± 1.91E-2	3.80E-3 ± 2.00E-3
DTM mortality	UEZ	2.54E-2 ± 2.04E-2	1.15E-3 ± 1.06E-3
NO3 uptake by FLAG	UEZ	0.193 ± 0.151	0.421 ± 0.251
NH4 uptake by FLAG	UEZ	1.192 ± 0.296	0.575 ± 0.301
FLAG ==> MIC FLAG ==> HERBnvm	UEZ UEZ	1.001 ± 0.17 0.034 ± 0.027	0.418 ± 0.09 0.087 ± 0.058
FLAG ==> HERBVM	UEZ	0.034 ± 0.027 0.034 ± 0.029	0.087 ± 0.038 0.1 ± 0.076
FLAG ==> APP	UEZ	1.74E-4 ± 1.50E-4	2.66E-4 ± 2.24E-4
FLAG ==> CLAD	UEZ	7.69E-5 ± 6.65E-5	1.53E-4 ± 1.20E-4
FLAG ==> nvmCAL	UEZ	0.063 ± 0.055	0.147 ± 0.101
FLAG ==> vmCAL	UEZ	0.042 ± 0.033	0.147 ± 0.084
DON exudation by FLAG	UEZ	0.391 ± 0.143	0.284 ± 0.103
FLAG mortality	UEZ	0.102 ± 0.066	0.106 ± 0.073
HNF ==> MIC	UEZ	0.137 ± 0.121	0.087 ± 0.085
HNF ==> APP	UEZ	1.63E-4 ± 1.45E-4	2.50E-4 ± 2.18E-4
HNF ==> HERBnvm	UEZ	0.041 ± 0.03	0.065 ± 0.054
HNF ==> HERBvm	UEZ	0.144 ± 0.103	0.646 ± 0.371
HNF ==> CLAD	UEZ	7.28E-5 ± 6.42E-5	1.40E-4 ± 1.13E-4
HNF ==> nvmCAL	UEZ	0.194 ± 0.139	0.266 ± 0.18
HNF ==> vmCAL	UEZ	0.111 ± 0.074 0.495 ± 0.127	0.336 ± 0.237 0.802 ± 0.176
HNF NH₄ excretion HNF DON excretion	UEZ UEZ	0.495 ± 0.127 0.295 ± 0.094	0.454 ± 0.111
HNF egestion	UEZ	0.625 ± 0.296	1.074 ± 0.304
MIC ==> HERBnvm	UEZ	0.044 ± 0.031	0.076 ± 0.058
MIC ==> HERBvm	UEZ	0.198 ± 0.123	0.46 ± 0.283
MIC ==> CLAD	UEZ	6.71E-5 ± 5.99E-5	1.43E-4 ± 1.16E-4
MIC ==> nvmCAL	UEZ	0.246 ± 0.141	0.238 ± 0.158
MIC ==> vmCAL	UEZ	0.131 ± 0.077	0.329 ± 0.214
MIC ==> PREFLEX	UEZ	3.73E-7 ± 1.57E-7	1.15E-8 ± 6.39E-9
MIC ==> POSTFLEX	UEZ	5.49E-6 ± 8.86E-7	1.25E-8 ± 6.61E-9
MIC NH4 excretion	UEZ	0.527 ± 0.12	0.656 ± 0.159
MIC DON excretion	UEZ	0.319 ± 0.094	0.376 ± 0.105
MIC egestion	UEZ	0.711 ± 0.301	0.865 ± 0.27
HERBnvm ==> CHAETO	UEZ	0.012 ± 0.01	0.026 ± 0.02
HERBnvm ==> POECIL	UEZ	0.012 ± 0.01	0.022 ± 0.017
HERBnvm ==> GELPRED	UEZ	0.012 ± 0.01	0.023 ± 0.019
		17	

		0.040 . 0.04	0.040 . 0.046
HERBnvm ==> PLANKFISH	UEZ	0.012 ± 0.01	0.018 ± 0.016
HERBnvm NH4 excretion	UEZ	0.042 ± 0.01	0.074 ± 0.018
HERBnvm DON excretion	UEZ	0.023 ± 0.007	0.042 ± 0.012
HERBnvm egestion	UEZ	0.033 ± 0.012	0.073 ± 0.026
APP ==> CHAETO	UEZ	9.42E-5 ± 8.12E-5	1.37E-4 ± 1.18E-4
APP ==> POECIL	UEZ	9.42E-5 ± 8.04E-5	1.35E-4 ± 1.17E-4
APP ==> GELPRED	UEZ	9.35E-5 ± 7.93E-5	1.35E-4 ± 1.16E-4
APP ==> PLANKFISH	UEZ	9.33E-5 ± 7.94E-5	1.35E-4 ± 1.17E-4
APP ==> PREFLEX	UEZ	8.43E-7 ± 3.06E-7	4.87E-8 ± 2.64E-8
APP ==> POSTFLEX	UEZ	6.77E-6 ± 4.72E-7	1.89E-6 ± 1.97E-7
APP NH4 excretion	UEZ	3.15E-4 ± 9.05E-5	5.00E-4 ± 1.50E-4
APP DON excretion	UEZ	1.68E-4 ± 5.43E-5	2.58E-4 ± 9.01E-5
APP egestion	UEZ	2.41E-4 ± 9.88E-5	3.74E-4 ± 1.56E-4
5			
CLAD ==> CHAETO	UEZ	2.64E-5 ± 2.15E-5	4.98E-5 ± 4.16E-5
CLAD ==> POECIL	UEZ	2.65E-5 ± 2.17E-5	5.00E-5 ± 4.10E-5
CLAD ==> GELPRED	UEZ	2.67E-5 ± 2.17E-5	4.87E-5 ± 4.09E-5
CLAD ==> PLANKFISH	UEZ	2.67E-5 ± 2.16E-5	4.93E-5 ± 4.11E-5
CLAD ==> PREFLEX	UEZ	2.20E-7 ± 1.31E-7	8.71E-7 ± 2.44E-7
CLAD ==> POSTFLEX	UEZ	2.35E-5 ± 2.25E-6	2.70E-5 ± 2.76E-6
CLAD NH4 excretion	UEZ	1.14E-4 ± 2.69E-5	2.22E-4 ± 5.41E-5
CLAD DON excretion	UEZ	6.27E-5 ± 1.75E-5	1.20E-4 ± 3.53E-5
CLAD egestion	UEZ	8.40E-5 ± 3.03E-5	1.49E-4 ± 5.60E-5
_			
nvmCAL ==> CHAETO	UEZ	0.079 ± 0.047	0.088 ± 0.067
nvmCAL ==> POECIL	UEZ	0.039 ± 0.025	0.025 ± 0.02
nvmCAL ==> GELPRED	UEZ	0.068 ± 0.041	0.055 ± 0.048
nvmCAL ==> PLANKFISH	UEZ	0.051 ± 0.037	0.051 ± 0.04
nvmCAL ==> PREFLEX	UEZ	4.75E-6 ± 1.24E-6	2.07E-6 ± 3.31E-7
nvmCAL ==> POSTFLEX	UEZ	6.37E-5 ± 9.63E-7	1.35E-5 ± 3.24E-7
nvmCAL NH4 excretion	UEZ	0.176 ± 0.031	0.169 ± 0.04
nvmCAL DON excretion	UEZ	0.1 ± 0.024	0.096 ± 0.027
nvmCAL egestion	UEZ	0.21 ± 0.059	0.223 ± 0.08
CHAETO ==> GELPRED	UEZ	0.029 ± 0.019	
			0.124 ± 0.074
CHAETO ==> PLANKFISH	UEZ	0.034 ± 0.02	0.057 ± 0.042
CHAETO NH4 excretion	UEZ	0.061 ± 0.021	0.146 ± 0.041
CHAETO DON excretion	UEZ	0.026 ± 0.015	0.046 ± 0.028
CHAETO egestion	UEZ	0.057 ± 0.025	0.21 ± 0.068
POECIL ==> GELPRED	UEZ		1.78E-2 ± 7.41E-3
		1.03E-2 ± 7.15E-3	
POECIL ==> PLANKFISH	UEZ	0.033 ± 0.017	0.019 ± 0.011
POECIL ==> PREFLEX	UEZ	1.22E-8 ± 6.56E-9	1.24E-8 ± 6.40E-9
POECIL ==> POSTFLEX	UEZ	2.76E-6 ± 1.84E-6	8.93E-7 ± 3.11E-8
POECIL NH4 excretion	UEZ	0.049 ± 0.014	0.037 ± 0.01
POECIL DON excretion	UEZ	0.017 ± 0.01	0.014 ± 0.007
POECIL egestion	UEZ	0.062 ± 0.022	0.037 ± 0.014
GELPRED ==> HTL	UEZ	0.044 ± 0.016	0.134 ± 0.057
GELPRED NH4 excretion	UEZ	0.049 ± 0.022	0.112 ± 0.046
GELPRED DON excretion			
	UEZ	0.02 ± 0.004	0.046 ± 0.022
GELPRED egestion	UEZ	0.054 ± 0.025	0.216 ± 0.089
PLANKFISH ==> HTL	UEZ	0.044 ± 0.02	0.065 ± 0.032
PLANKFISH NH4 excretion	UEZ	0.067 ± 0.031	0.091 ± 0.039
PLANKFISH DON excretion	UEZ	0.027 ± 0.012	0.041 ± 0.023
PLANKFISH egestion	UEZ	0.062 ± 0.027	0.093 ± 0.044
PREFLEX growth	UEZ	6.86E-7 ± 4.83E-7	3.22E-7 ± 2.34E-7
PREFLEX mortality	UEZ	6.76E-7 ± 4.75E-7	3.52E-7 ± 2.35E-7
PREFLEX NH4 excretion	UEZ	2.08E-6 ± 7.07E-7	1.07E-6 ± 3.10E-7
PREFLEX DON excretion	UEZ	1.10E-6 ± 4.11E-7	5.50E-7 ± 1.86E-7
PREFLEX egestion	UEZ	1.66E-6 ± 7.28E-7	7.18E-7 ± 3.06E-7
POSTFLEX growth	UEZ	1.14E-5 ± 7.36E-6	4.82E-6 ± 3.17E-6
POSTFLEX mortality	UEZ	1.14E-5 ± 7.43E-6	4.90E-6 ± 3.18E-6
POSTFLEX NH4 excretion	UEZ	3.32E-5 ± 9.10E-6	1.39E-5 ± 3.74E-6
POSTFLEX DON excretion	UEZ	1.77E-5 ± 5.41E-6	7.47E-6 ± 2.29E-6
POSTFLEX egestion	UEZ	2.84E-5 ± 1.05E-5	1.22E-5 ± 4.38E-6
BAC ==> FLAG	UEZ	0.297 ± 0.144	0.322 ± 0.165
BAC ==> HNF	UEZ	0.173 ± 0.137	0.294 ± 0.199
	UEZ	0.125 ± 0.109	
BAC ==> MIC			0.309 ± 0.201
BAC ==> APP	UEZ	1.25E-4 ± 1.05E-4	2.71E-4 ± 2.16E-4
BAC NH4 excretion	UEZ	1.608 ± 0.223	2.329 ± 0.199
DOM uptake by BAC	UEZ	2.203 ± 0.305	3.254 ± 0.277
•			
		1 ♀	

sDET ==> HNF	UEZ	1.407 ± 0.585	2.479 ± 1.023
sDET ==> MIC	UEZ	0.609 ± 0.462	1.297 ± 0.9
sDET ==> APP	UEZ	1.82E-4 ± 1.55E-4	2.47E-4 ± 2.11E-4
sDET dissolution to DOM	UEZ	0.15 ± 0.136	0.091 ± 0.091
IDET ==> HERBnvm	UEZ	0.024 ± 0.021	0.049 ± 0.044
IDET ==> CLAD	UEZ	4.97E-5 ± 4.41E-5	1.44E-4 ± 1.15E-4
IDET ==> nvmCAL	UEZ	0.214 ± 0.107	0.053 ± 0.039
IDET ==> HERBvm	UEZ	0.056 ± 0.041	0.21 ± 0.171
IDET ==> vmCAL	UEZ	0.039 ± 0.031	0.109 ± 0.106
IDET dissolution to DOM	UEZ	0.042 ± 0.04	0.035 ± 0.036
HERBvm ==> CHAETO	UEZ	0.056 ± 0.044	0.241 ± 0.149
HERBvm ==> POECIL	UEZ	0.041 ± 0.031	0.036 ± 0.027
HERBvm ==> GELPRED	UEZ	0.031 ± 0.022	0.142 ± 0.109
HERBym ==> PLANKFISH	UEZ	0.04 ± 0.025	0.072 ± 0.061
HERBym NH4 excretion	UEZ	0.087 ± 0.035	0.278 ± 0.077
HERBym DOM excretion	UEZ	0.031 ± 0.024	0.13 ± 0.059
HERBym egestion	UEZ	0.04 ± 0.026	0.269 ± 0.151
HERBvm ==> CHAETO	DCM	0.034 ± 0.022	0.092 ± 0.082
HERBym ==> POECIL	DCM	0.03 ± 0.015	0.092 ± 0.002
HERBym ==> GELPRED	DCM	0.03 ± 0.013 0.024 ± 0.01	0.086 ± 0.077
HERBym ==> PLANKFISH	DCM	0.024 ± 0.01 0.023 ± 0.022	0.052 ± 0.048
HERBym NH4 excretion	DCM	0.023 ± 0.022 0.034 ± 0.029	0.032 ± 0.048 0.038 ± 0.036
HERBym DOM excretion	DCM		
		0.043 ± 0.022	0.055 ± 0.046
HERBym egestion	DCM	0.033 ± 0.025	0.098 ± 0.094
HERBym NH4 excretion	Twilight	0.03 ± 0.016	0.108 ± 0.048
HERBym DOM excretion	Twilight	0.017 ± 0.011	0.05 ± 0.029
HERBym egestion	Twilight	0.027 ± 0.008	0.051 ± 0.049
HERBvm Mortality	Twilight	0.02 ± 0.011	0.058 ± 0.056
vmCAL ==> CHAETO	UEZ	0.06 ± 0.039	0.226 ± 0.135
vmCAL ==> POECIL	UEZ	0.079 ± 0.037	0.041 ± 0.028
vmCAL ==> GELPRED	UEZ	0.017 ± 0.006	0.147 ± 0.123
vmCAL ==> PLANKFISH	UEZ	0.03 ± 0.028	0.074 ± 0.064
vmCAL NH4 excretion	UEZ	0.077 ± 0.034	0.321 ± 0.084
vmCAL DOM excretion	UEZ	0.035 ± 0.019	0.157 ± 0.066
vmCAL egestion	UEZ	0.048 ± 0.028	0.432 ± 0.239
vmCAL ==> CHAETO	DCM	0.006 ± 0.004	0.107 ± 0.091
vmCAL ==> POECIL	DCM	0.008 ± 0.004	0.121 ± 0.098
vmCAL ==> GELPRED	DCM	0.004 ± 0.003	0.098 ± 0.089
vmCAL ==> PLANKFISH	DCM	0.042 ± 0.005	0.051 ± 0.046
vmCAL NH4 excretion	DCM	0.032 ± 0.026	0.038 ± 0.037
vmCAL DOM excretion	DCM	0.025 ± 0.017	0.053 ± 0.045
vmCAL egestion	DCM	0.012 ± 0.007	0.122 ± 0.107
vmCAL NH4 excretion	Twilight	0.027 ± 0.015	0.135 ± 0.057
vmCAL DOM excretion	Twilight	0.016 ± 0.009	0.06 ± 0.033
vmCAL egestion	Twilight	0.032 ± 0.02	0.055 ± 0.053
vmCAL Mortality	Twilight	0.015 ± 0.013	0.058 ± 0.059
Sinking DTM	UEZ==>DCM	2.29E-2 ± 1.33E-2	4.93E-3 ± 2.29E-3
Sinking FLAG	UEZ==>DCM	0.016 ± 0.012	0.029 ± 0.015
Sinking IDET	UEZ==>DCM	1.59E-1 ± 9.17E-2	1.00E+0 ± 7.35E-2
Upwelled NO₃	DCM	0.036 ± 0.035	0.022 ± 0.022
Lateral Input of DON	DCM	0.068 ± 0.064	0.038 ± 0.036
Lateral Input of PON	DCM	0.414 ± 0.155	0.559 ± 0.272
Nitrification	DCM	1.131 ± 0.424	0.215 ± 0.077
N ₂ fixation by PICO	DCM	0.027 ± 0.027	0.019 ± 0.019
NO₃ uptake by PICO	DCM	0.598 ± 0.413	0.107 ± 0.077
NH₄ uptake by PICO	DCM	0.94 ± 0.428	1.682 ± 0.177
PICO ==> HNF	DCM	0.242 ± 0.117	0.256 ± 0.117
PICO ==> MIC	DCM	0.085 ± 0.074	0.082 ± 0.072
PICO ==> FLAG	DCM	0.114 ± 0.088	0.088 ± 0.069
PICO ==> APP	DCM	0.321 ± 0.125	0.528 ± 0.161
DON exudation by TRICHO	DCM	0.583 ± 0.112	0.685 ± 0.099
TRICHO mortality	DCM	0.221 ± 0.071	0.168 ± 0.138
N2 fixation by TRICHO	DCM	4.12E-5 ± 2.85E-5	6.42E-6 ± 4.53E-6
NO3 uptake by TRICHO	DCM	5.30E-5 ± 3.74E-5	7.51E-6 ± 5.43E-6
NH4 uptake by TRICHO	DCM	5.04E-5 ± 3.63E-5	7.64E-6 ± 5.47E-6
DON exudation by TRICHO	DCM	8.10E-5 ± 4.58E-5	1.05E-5 ± 6.67E-6
TRICHO mortality	DCM	6.36E-5 ± 4.05E-5	1.10E-5 ± 6.74E-6
-,	-	10	

NO3 uptake by DTM	DCM	3.90E-2 ± 2.52E-2	4.24E-3 ± 2.64E-3
NH4 uptake by DTM	DCM	3.80E-2 ± 2.48E-2	4.16E-3 ± 2.70E-3
DTM ==> MIC	DCM	6.75E-3 ± 4.36E-3	3.05E-3 ± 8.71E-4
DTM ==> HERBnvm	DCM	9.72E-3 ± 8.92E-3	1.05E-3 ± 1.00E-3
DTM ==> HERBvm	DCM	9.41E-3 ± 8.83E-3	1.04E-3 ± 9.93E-4
DTM ==> APP	DCM	9.01E-3 ± 8.38E-3	1.03E-3 ± 9.91E-4
DTM ==> CLAD	DCM	9.95E-3 ± 9.10E-3	1.03E-3 ± 9.83E-4
DTM ==> nvmCAL	DCM	1.00E-2 ± 9.36E-3	1.03E-3 ± 9.86E-4
DTM ==> vmCAL	DCM	8.71E-3 ± 8.37E-3	1.02E-3 ± 9.91E-4
DON exudation by DTM	DCM	1.85E-2 ± 1.00E-2	1.98E-3 ± 1.07E-3
DTM mortality	DCM	1.07E-2 ± 5.78E-3	1.06E-3 ± 9.44E-4
NO3 uptake by FLAG	DCM	0.53 ± 0.319	0.126 ± 0.081
NH4 uptake by FLAG	DCM	0.596 ± 0.352	0.363 ± 0.148
FLAG ==> MIC	DCM	0.589 ± 0.128	0.039 ± 0.019
FLAG ==> HERBnvm	DCM	0.079 ± 0.063	0.079 ± 0.061
FLAG ==> HERBvm	DCM	0.045 ± 0.041	0.075 ± 0.065
FLAG ==> APP	DCM	0.054 ± 0.05	0.043 ± 0.04
FLAG ==> CLAD	DCM	0.092 ± 0.071	0.087 ± 0.067
FLAG ==> nvmCAL	DCM	0.092 ± 0.071 0.097 ± 0.073	0.094 ± 0.07
FLAG ==> vmCAL	DCM	0.044 ± 0.04	0.078 ± 0.068
DON exudation by FLAG	DCM	0.35 ± 0.093	0.142 ± 0.055
FLAG mortality	DCM	0.127 ± 0.068	0.078 ± 0.047
HNF ==> MIC	DCM	0.045 ± 0.043	0.034 ± 0.032
HNF ==> APP	DCM	0.043 ± 0.041	0.031 ± 0.03
HNF ==> HERBnvm	DCM	0.069 ± 0.058	0.052 ± 0.043
HNF ==> HERBvm	DCM	0.028 ± 0.029	0.106 ± 0.076
HNF ==> CLAD	DCM	0.083 ± 0.066	0.043 ± 0.039
HNF ==> nvmCAL	DCM	0.07 ± 0.058	0.047 ± 0.042
HNF ==> vmCAL	DCM	0.039 ± 0.035	0.053 ± 0.054
HNF NH ₄ excretion	DCM	0.244 ± 0.069	0.224 ± 0.066
HNF DON excretion	DCM	0.142 ± 0.045	0.128 ± 0.04
HNF egestion	DCM	0.306 ± 0.128	0.295 ± 0.113
MIC ==> HERBnvm	DCM	0.105 ± 0.076	0.055 ± 0.047
MIC ==> HERBvm	DCM	0.063 ± 0.051	0.056 ± 0.053
MIC ==> CLAD	DCM	0.108 ± 0.081	0.045 ± 0.04
MIC ==> nvmCAL	DCM	0.101 ± 0.075	0.047 ± 0.041
MIC ==> vmCAL	DCM	0.071 ± 0.044	0.05 ± 0.045
MIC NH4 excretion	DCM	0.287 ± 0.064	0.168 ± 0.052
MIC DON excretion	DCM	0.167 ± 0.046	0.098 ± 0.034
MIC egestion	DCM	0.373 ± 0.122	0.216 ± 0.093
HERBnvm ==> CHAETO	DCM	0.045 ± 0.027	0.023 ± 0.019
HERBnvm ==> POECIL	DCM	0.046 ± 0.027	0.023 ± 0.013
HERBnvm ==> GELPRED	DCM	0.037 ± 0.034	0.025 ± 0.023
HERBnvm ==> PLANKFISH	DCM	0.032 ± 0.029	0.024 ± 0.022
HERBnvm NH4 excretion	DCM	0.119 ± 0.037	0.077 ± 0.026
HERBnvm DON excretion	DCM	0.135 ± 0.071	0.088 ± 0.044
HERBnvm egestion	DCM	0.069 ± 0.025	0.045 ± 0.017
APP ==> CHAETO	DCM	0.078 ± 0.058	0.087 ± 0.067
APP ==> POECIL	DCM	0.08 ± 0.059	0.087 ± 0.066
APP ==> GELPRED	DCM	0.055 ± 0.047	0.069 ± 0.059
APP ==> PLANKFISH	DCM	0.049 ± 0.044	0.055 ± 0.048
APP NH4 excretion	DCM	0.142 ± 0.048	0.111 ± 0.036
APP DON excretion	DCM	0.073 ± 0.032	0.059 ± 0.025
APP egestion	DCM	0.273 ± 0.092	0.381 ± 0.107
CLAD ==> CHAETO	DCM	0.041 ± 0.033	0.028 ± 0.025
CLAD ==> POECIL			
	DCM	0.039 ± 0.032	0.027 ± 0.022
CLAD ==> GELPRED	DCM	0.029 ± 0.027	0.026 ± 0.024
CLAD ==> PLANKFISH	DCM	0.022 ± 0.019	0.027 ± 0.023
CLAD NH4 excretion	DCM	0.099 ± 0.033	0.085 ± 0.029
CLAD DON excretion	DCM	0.048 ± 0.022	0.043 ± 0.02
CLAD egestion	DCM	0.114 ± 0.058	0.104 ± 0.052
nvmCAL ==> CHAETO	DCM	0.044 ± 0.039	0.028 ± 0.025
nvmCAL ==> POECIL	DCM	0.047 ± 0.04	0.029 ± 0.027
nvmCAL ==> GELPRED	DCM	0.037 ± 0.033	0.025 ± 0.023
nvmCAL ==> PLANKFISH	DCM	0.032 ± 0.03	0.024 ± 0.022
nvmCAL NH4 excretion	DCM	0.118 ± 0.039	0.083 ± 0.029
nvmCAL DON excretion	DCM	0.059 ± 0.025	0.041 ± 0.019
	DOIVI		5.0 11 2 0.013
		20	

nvmCAL egestion	DCM	0.14 ± 0.072	0.101 ± 0.052
CHAETO ==> GELPRED	DCM	0.04 ± 0.027	0.065 ± 0.047
CHAETO ==> PLANKFISH	DCM	0.034 ± 0.025	0.052 ± 0.041
CHAETO NH4 excretion	DCM	0.065 ± 0.024	0.064 ± 0.025
CHAETO DON excretion	DCM	0.036 ± 0.016	0.034 ± 0.016
CHAETO egestion	DCM	0.074 ± 0.035	0.149 ± 0.068
POECIL ==> GELPRED	DCM	0.04 ± 0.027	0.074 ± 0.051
POECIL ==> PLANKFISH	DCM	0.031 ± 0.024	0.056 ± 0.043
POECIL NH4 excretion	DCM	0.065 ± 0.025	0.062 ± 0.024
POECIL DON excretion	DCM	0.036 ± 0.016	0.033 ± 0.015
POECIL egestion	DCM	0.078 ± 0.036	0.164 ± 0.069
GELPRED ==> HTL	DCM	0.067 ± 0.026	0.14 ± 0.059
GELPRED NH4 excretion	DCM	0.07 ± 0.024	0.085 ± 0.028
GELPRED DON excretion	DCM	0.037 ± 0.016	0.044 ± 0.02
GELPRED egestion	DCM	0.091 ± 0.039	0.2 ± 0.076
PLANKFISH ==> HTL	DCM	0.049 ± 0.024	0.072 ± 0.033
PLANKFISH NH4 excretion	DCM	0.08 ± 0.029	0.086 ± 0.03
PLANKFISH DON excretion	DCM	0.041 ± 0.019	0.045 ± 0.02
PLANKFISH egestion	DCM	0.095 ± 0.041	0.139 ± 0.054
BAC ==> FLAG	DCM	0.237 ± 0.121	0.17 ± 0.098
BAC ==> HNF	DCM	0.102 ± 0.095	0.101 ± 0.08
BAC ==> MIC	DCM	0.082 ± 0.073	0.098 ± 0.076
BAC ==> APP	DCM	0.12 ± 0.088	0.092 ± 0.071
BAC NH4 excretion	DCM	1.35 ± 0.125	1.142 ± 0.102
DOM uptake by BAC	DCM	1.89 ± 0.175	1.603 ± 0.144
sDET ==> HNF	DCM	0.726 ± 0.359	0.656 ± 0.353
sDET ==> MIC	DCM	0.468 ± 0.283	0.479 ± 0.248
sDET ==> APP	DCM	0.203 ± 0.152	0.152 ± 0.131
sDET dissolution to DOM	DCM	0.044 ± 0.044	0.031 ± 0.03
IDET ==> HERBnvm	DCM	0.22 ± 0.155	0.122 ± 0.097
IDET ==> CLAD	DCM	0.1 ± 0.096	0.163 ± 0.117
IDET ==> nvmCAL	DCM	0.199 ± 0.148	0.143 ± 0.112
IDET ==> HERBvm	DCM	0.049 ± 0.038	0.3 ± 0.224
IDET ==> vmCAL	DCM	0.066 ± 0.049	1.189 ± 0.384
IDET dissolution to DOM	DCM	0.049 ± 0.045	0.028 ± 0.028
Sinking DTM	DCM==>Twilight	0.007 ± 0.006	0.001 ± 0.001
Sinking FLAG	DCM==>Twilight	0.016 ± 0.01	0.057 ± 0.031
Sinking IDET	DCM==>Twilight	0.436 ± 0.026	0.465 ± 0.178